DEVELOPMENT OF AN OPTICAL DISC RECORDER

QUARTERLY TECHNICAL REPORT

July 1 to September 30, 1976

Sponsored by

ADVANCED RESEARCH PROJECTS AGENCY

ARPA Order No. 3080
Program Code No. 6D30

Contract No. N00014-76-C-0441

Principal Investigator: George Kenney (914) 762-0300
Scientific Officer: Marvin Denicoff

Amount of Contract: $700,719
Contract Period: 1 Oct. 1975 - 31 March 1977
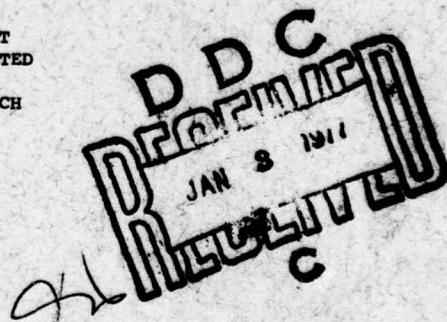
Prepared by

PHILIPS LABORATORIES

A Division of North American Philips Corporation
Briarcliff Manor, New York 10510

November 1976
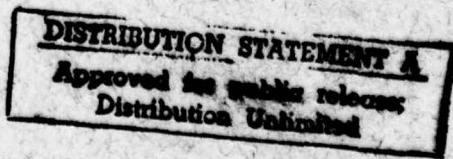
| REPORT DOCUMENTATION PAGE | | READ INSTRUCTIONS BEFORE COMPLETING FORM |
|---|---|---|
| 1. REPORT NUMBER | 2. GOVT ACCESSION NO. | 3. RECIPIENT'S CATALOG NUMBER |
| 4. TITLE (and Subtitle) DEVELOPMENT OF AN OPTICAL DISC RECORDER | | 5. TYPE OF REPORT & PERIOD COVERED Quarterly Technical Report. 1 July 1976 — 30 Sept 1976 |
| | | 6. PERFORMING ORG. REPORT NUMBER PL-52-VR-1124 |
| 7. AUTHOR(s) G. Kenney, F. Zernike, D. Lou, M. Goutmann, A. Milch, D. Stanton, M. Strzelczyk, R. Hunt, J. Wagner, A. Chan, R. McFarlane | | 8. CONTRACT OR GRANT NUMBER(s) N00014-76-C-0441, ARPA Order 3080 |
| 9. PERFORMING ORGANIZATION NAME AND ADDRESS Philips Laboratories A Division of North American Philips Corp. Briarcliff Manor, New York 10510 | | 10. PROGRAM ELEMENT, PROJECT, TASK AREA & WORK UNIT NUMBERS ARPA Order No. 3080 Program Code No. 6D30 |
| 11. CONTROLLING OFFICE NAME AND ADDRESS Advanced Research Projects Agency 1400 Wilson Blvd. Arlington, Virginia 22209 | | 12. REPORT DATE November 1976 |
| | | 13. NUMBER OF PAGES 98 |
| 14. MONITORING AGENCY NAME & ADDRESS(if different from Controlling Office) Office of Naval Research 800 North Quincy Street Arlington, Virginia 22217 Code: 437 | | 15. SECURITY CLASS. (of this report) UNCLASSIFIED |
| | | 15a. DECLASSIFICATION/DOWNGRADING SCHEDULE |

16. DISTRIBUTION STATEMENT (of this Report)

Approved for public release. Distribution unlimited.

17. DISTRIBUTION STATEMENT (of the abstract entered in Block 20, if different from Report)

18. SUPPLEMENTARY NOTES

19. KEY WORDS (Continue on reverse side if necessary and identify by block number)

opitcal disc recorder
direct read after write (DRAW)
lasers
substrate materials

recording materials
disc protective mechanism
disc

20. ABSTRACT (Continue on reverse side if necessary and identify by block number) The recorder was modified for limited operation at 3 rps. Refitting the new optical and digital subsystems into a deliverable system is now planned on a back-up sled and turntable. PMMA discs coated with tellurium films were recorded on through the backside of the disc surface. Air sandwich fabrication is showing good progress. First results of an accelerated life testing program indicate that tellurium films do not degrade at high temperatures. An initial recommendation for digital formatting, coding, and error correction techniques is given. A theoretical analysis of expected hole machining characteristics for a moving substrate was performed.

DD FORM 1 JAN 73 1473   EDITION OF 1 NOV 65 IS OBSOLETE

384334

PHILIPS LABORATORIES

## TABLE OF CONTENTS

iii

QUARTERLY TECHNICAL REPORT

1 July 1976 to 30 September 1976

## 1.    SUMMARY

The recorder was modified for limited operation at 3 rps.  Debugging of the playback optical system is still in progress.
So as not to disrupt experiments on this recorder, refitting with
the new optical and digital subsystems into a deliverable system
is now planned on what was originally intended as a back-up sled
and turntable.  PMMA discs coated with tellurium films were written
on with the N.V. Philips (NVP) machine.  Recording was done through
the backside  of the disc surface using a new objective.  Air sandwich fabrication is showing good progress.  First results of an
accelerated life testing program indicate that tellurium films do
not degrade at high temperatures and may be archival.  An initial
recommendation for digital formatting, coding, and error correction techniques is given.  A theoretical analysis of expected hole
machining characteristics for a moving substrate was performed.

## 2.    RESEARCH PROGRAM OBJECTIVES

The objective of this program is to develop an optical disc
recorder of digital information, with a $\underline{d}$irect-$\underline{r}$ead-$\underline{a}$fter-$\underline{w}$rite
(DRAW) capability.  A storage capacity of $> 10^{10}$ bits is
desired, with $4.4 \times 10^5$ bits on each of the 40,000 tracks of
the disc.  The desired error rate is $10^{-9}$ at a data rate
greater than 1.33 Mbit/sec.  The key element in the proposed
system is a recording material that can be exposed with a low-
power laser (e.g., HeNe), leading to a recorder that could be
manufactured for < \$10,000 and discs that would cost < \$10 in
quantity.

## 3.    SCHEDULE

The program schedule and milestones given in Figure 1 are for
both materials development and recorder construction.  Difficulties with the optical-focus motor and the playback optics

**TASK**

**MATERIALS**

1.

1.1 Perform static eval. of sensitivity (Bi, AsSe₃, Sb, Cd, Te, Se)

1.2 Produce in-house discs

1.3 Evaluate S/N, defects, etc., with operating recorder

1.4 Develop disc protective-mechanism interface

1.5 Finalize disc design.

1.6 Archival testing Te & Bi

**RECORDER**

2.

2.1 Construct DRAW recorder based on analog VLP machine with argon write laser & HeNe read laser

· Recorder tests with PRL discs

· Recorder tests with PL discs

2.2 Dev. digital electronics subsystem

2.3 Dev. low-power optical subsystem

2.4 Dev. ultra-slow radial sled

2.5 Refit recorder with final subsystem

2.6 Test & evaluate recorder

· Parametric system studies (pwr: 5-80 mW; speed: 1-15 rps)

▲ Completed tasks.

Figure 1:  Program Schedule for Development of Optical Disc Recorder

(sht. 1 of 2)

1976 — 1977

J F M A M J J A S O N D J F M A M J

1976    1977

J F M A M J J A S O N D J F M A M J

TASK

**PROGRAM MILESTONES**

| Milestone No. | Description |
| --- | --- |
| 1 | First narrowing of material choices complete. |
| 2 | large-area deposition capability available. |
| 3 | Second narrowing of material choices complete. |
| 4 | Optimum material selected. |
| 5 | Deliverable discs available. |
| 6 | Recorder available for test. |
| 7a | Characterization of recorder channel complete. |
| 7b | Assy. of digital electronics subsystem complete. |
| 8 | Assy. of optical subsystem complete. |
| 9 | Assy. of improved radial sled complete. |
| 10 | Final system assembly and checkout complete. |
| 11 | Deliver laboratory prototype system. |
| 12 | Parametric system studies completed. |
| 13 | First lifetests on tellurium available. |
| 14 | First archival results tellurium & bismuth. |

Figure 1: Program Schedule for Development of Optical Disc Recorder    (sht. 2 of 2)

and servo systems have delayed testing of the disc with the re-
corder. The recorder should be operational in the next quarter.
In order not to delay the materials program, however, testing
of discs made at NVP and PL (Task 1.3) is underway with the NVP
recorder. The quality of large-area deposition of tellurium is
now satisfactory for fair quality video recording which infers
acceptable quality for digital recording. Based on these re-
sults and expected tests in October, we still expect to narrow
the material choice in October.

A new task to investigate the archival properties of tellurium
and bismuth films was initiated (Task 1.6). Milestone 13 of
this task was met; the results of the first life tests of tel-
lurium are given in Appendix D. Results sufficient to deter-
mine the archival properties based on accelerated high temper-
ature aging (milestone 14) are expected by January 1, 1977.

A second set of data on the channel error characteristics was
received from NVP. Based on the data, Magnavox has recommended
a coding and error correction technique. It is expected that
the initial characterization of the recorder channel will be com-
pleted on schedule in late October (milestone 7a).

A re-examination of the proposed refitting program (Task 2.5)
has resulted in some schedule changes. So as not to disrupt
anticipated experiments on the PL recorder, refitting of the
new optical subsystem (Task 2.3) and the digital electronics
subsystem into the deliverable system (Task 2.2) is now planned
on a back-up sled and turntable. This should allow both efforts
to proceed without interference. The refitted recorder is now
planned for February 1, 1977 (Task 2.5). The three-month test
and evaluation of the recorder (Task 2.6) is still planned and
should be completed by April 30, 1977.

## 4.    PROGRESS AND DISCUSSION

### 4.1    Focus System

The focusing motor of the recorder has a limited range which does not allow reliable operation with PMMA discs at 30 rps, the design speed on the analog VLP recorder (Task 2.1). Because the focusing system reads from above the disc, the need for a fail-safe mechanism to prevent the lens from crashing onto the disc surface complicates the design and limits the working range and maximum acceleration of the objective. Since it is not feasible to modify the focus motor to operate satisfactorily at 30 rps, an effort to reduce the disc rotation speed to the designed 3 rps was undertaken. The slower speed reduces by a factor of 100 the acceleration requirements of the focus motor. The required redesign of the servos for the turntable and focusing motors was completed and tested satisfactorily at 3 rps disc operation. Even this redesign will permit only limited recording capabilities using discs of excellent flatness.

As indicated above, however, recording and playback from the underside of the disc will relax the focus motor requirements and allow greater travel range and acceleration. However, before the design of a new focusing motor is attempted, it has been decided to evaluate existing motors to determine their frequency response and travel capabilities. These results will be compared with the expected requirements, derived from disc measurements, and used as a basis for a new focus motor design.

The focus motors under consideration include those from the PL machine, the NVP machine, and from the VLP player (integrator-type). Evaluation of the frequency response of the integrator player motor was completed and has revealed a resonance at about 12 kHz and a slight resonance at 100 Hz. Since it is expected that the motor will be required to follow motion of less than a few kHz, it may be concluded that the high frequency resonance

would not be a significant problem. The resonance at 100 Hz is so slight that it would not be important. This motor transports a lens which weighs about 4 grams. Some preliminary tests of the PL focusing motor have indicated a possible resonance at 2 kHz, possibly due to the spring suspension of the lens. This may be a limitation for higher disc speeds. When a complete characterization of these three motors has been made, and possibly of some spring-suspended, non-air bearing motors which are also available, a new design will be formulated. We will thus avoid any problems discovered in existing motors and will design for motions as predicted by the disc measurements.

## 4.2    Sled

Work on the optical sled has involved the construction of a back-up sled to be used in the evaluation of fast access mechanisms (Fig. 2). This second sled is similar to that of the PL machine in that it uses the same linear motor, tachometer, and Dover air bearing with jeweled orifices. The linear motor is capable of producing a force of about 2 newtons and should be able to move the bearing collar over a travel of 10 cm in less than 1/2 second. Some preliminary tests have shown that the new air bearing is less subject to vibration than the unjeweled bearing, although it still shows a tendency to resonate at about 30 Hz. These results are still to be confirmed on the back-up sled assembly. A set of PL-type electronics designed to drive the sled at constant speeds has also been constructed and is ready for installation. Upon assembly of the sled, a vibration problem was discovered involving the tachometer mount. This problem should be solved, however, by only slight modification.

The sled will be used to evaluate the performance of the linear velocity transducer, as well as an accelerometer and an interferometer for use as speed and positioning control sensors. Based on these tests, the best combination of sensors will be incorporated into an improved sled design. It has also been decided

that the optics carried on the sled will be reduced to a focusing motor, and possibly a fixed mirror, and that reading and writing will be done from the underside of the disc. As a result of the latter consideration, the sled was built with a much lower profile, thereby reducing the possibility of vibrations. The height was reduced by about 8 cm and is compatible with the turntable currently being evaluated.
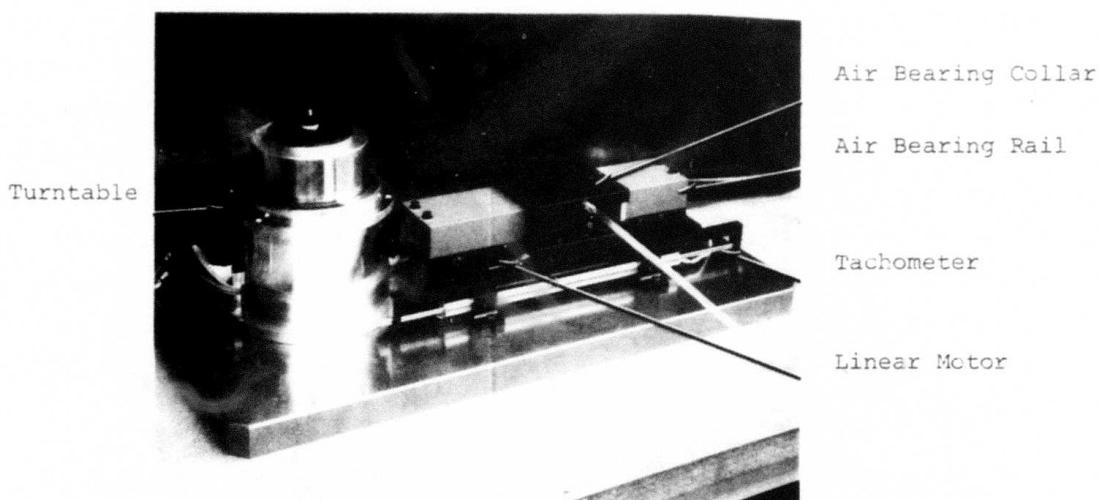


Figure 2: Fast access sled.

## 4.3    Air Bearing Turntables

The ac drive electronics for the back-up air bearing turntable (now to be part of the deliverable machine) were completed. The system is designed for 3, 10, and 30 Hz operation. Evaluation of the electro-mechanical characteristics of the turntable has begun.

A parallel effort to build a high-quality, air-bearing-based turntable from commercially available components was also initiated during the quarter. The bearing chosen was a Professional Instruments Model 4B; the manufacturer's specification is less than 0.05 μm wobble. The bearing will be directly driven by an integrally mounted PMI pancake armature motor. A 2000 line

optical tachometer with double pickoff will be used to monitor the speed. The bearing and a PMI Model W9M4M motor are currently being evaluated.

## 4.4    Materials Evaluation

A theoretical analysis to predict the characteristics of hole machining on a moving substrate has been carried out. The results are reported in Appendix C. The laser power required to machine a 2 μm x 1 μm pit at the outer edge of a rotating disc (30 cm diam.) is about twice that required for machining 1 μm diameter pits under static conditions. The calculations also suggest it may be proper to use lenses of much lower numerical aperture for optimum writing. A lens of low numerical aperture would have a longer depth-of-field, a wider field-of-view, and a lower mass. It is expected that this would simplify the demands on the tracking and focusing systems. Experiments are now underway to measure experimentally the optimum spot profile for writing on a moving substrate.

A technique (see Appendix A) has been developed to measure and align the spot profiles of the writing and reading laser beams on the disc. Large area (30 cm diam.) discs of tellurium of uniform thickness have been fabricated at PL. DRAW recording was done through the backside of the disc surface using a new (Cerco) objective. Figure 3 shows an optical micrograph of pits written with the Cerco objective on 250 Å of tellurium film deposited on a PMMA disc.

The frequency of the DRAW signal was 10 MHz square wave. The maximum laser power required for writing at the outer radius of the disc was less than 20 mW. Readback signal-to-noise was better than 30 dB; these results are detailed in Appendix G.

The spectral absorption of tellurium was measured and is reported in Appendix D. This data indicates that it is reasonable to extrapolate measurements of sensitivity at the 488 nm argon laser

wavelength into the 633 nm He-Ne laser and 850 nm GaAs laser
wavelengths.
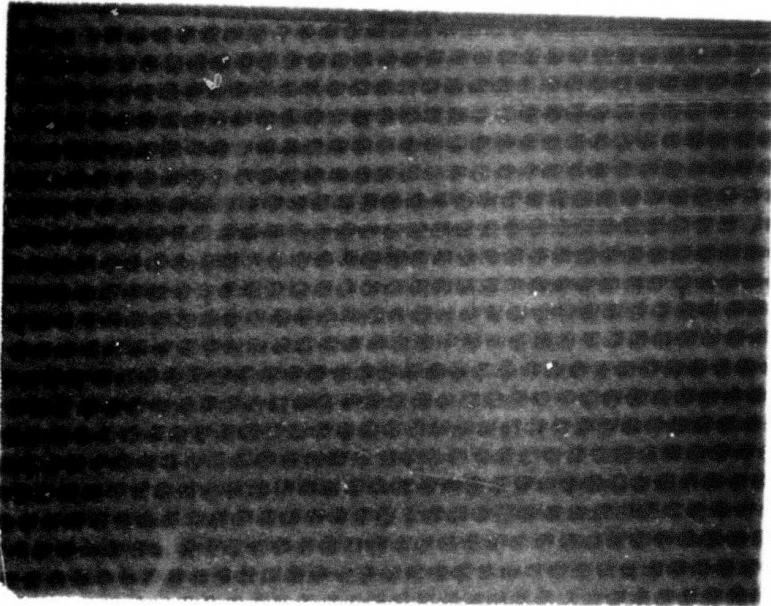


Figure 3:  Optical micrograph of recording on
Te film (250 Å thick).

## 4.5     Air Sandwich Assembly Fixture

A fixture for assembling air sandwich discs was fabricated (see
Fig. 4).  The assembly procedure  is as follows:  a substrate is
placed on the base plate, and the assembly is then rotated slowly
as adhesive is dispensed onto the substrate in the standoff zones.
Next, the inner and outer standoffs are guided into place on the
substrate.  The standoff guide is removed, and the assembly is
again rotated as adhesive i. dispensed onto the standoffs.  Finally
the upper substrate is lowered into position on the standoffs.
To minimize the droop of the upper substrate as the adhesive cures,
it is held flat by the vacuum hold-down plate.

Several air sandwiches were assembled.  The substrates were 1 mm
thick Glasflex Electroglas Sheet.  The standoffs were 0.4 mm
thick polyvinyl chloride; Eastman 910 was used as the adhesive.

9

Although one difficulty did arise, the results were encouraging.
The problem encountered was that of non-uniform spreading of the
adhesive during the lamination process.  This was attributed to
two factors:  variations in substrate thickness, and variations
in adhesive thickness between the inner and the outer standoff
zones.  It is felt that both of these difficulties can be success-
fully corrected by making the base plate surface more compliant,
and altering the ratio of adhesive dispensed in the two zones.
These two modifications are currently being incorporated.
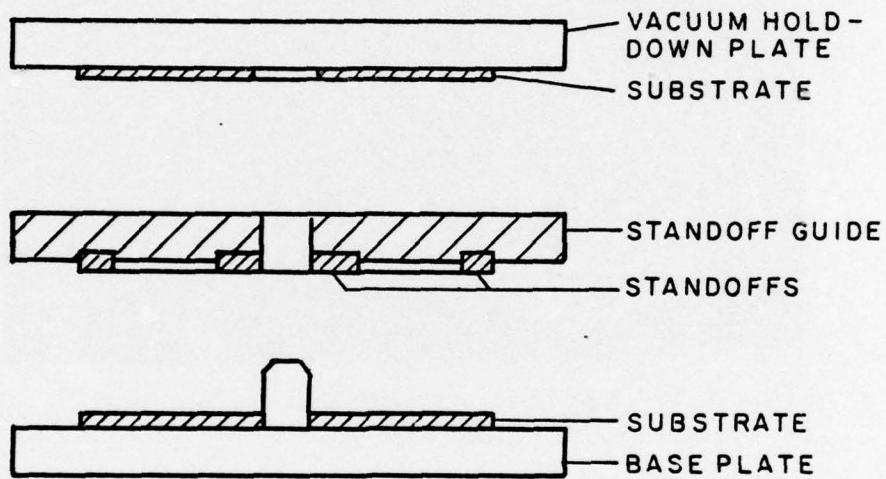


Figure 4:  Air Sandwich Assembly Fixture.

## 4.6    Substrate Material

To minimize chemical contamination of the as-received surfaces,
Glasflex PMMA sheet is currently being purchased in the un-
protected form.  As a result, the manufacturer is reluctant to
check the sheet thickness of the stock delivered.  Thickness
variations have been quite severe.  Measurements made about 2 cm
from the edge of nominally 30 cm square sheets range from 0.72
to 1.31 mm on the Glasflex homopolymer and 0.90 to 1.16 mm on
the copolymer.  In neither case was a wedge shape observed.
Recent measurement on several hundred squares on the homopolymer

indicate that 70% of them are out of specification (0.87 to
1.13 mm). Discussions are currently underway with Glasflex
Corporation on ways to remedy the problem.

In addition to the difficulty in assembling air sandwich discs
from sheet stock with such widely varying thickness, it has also
been difficult to maintain balance. A typical disc made from
the homopolymer described above is 55 gm-cm out of balance.
Alternately, the pre-protected homopolymer discs are only typi-
cally 6 gm-cm out of balance. It is interesting to note that in
both cases the imbalance of an air sandwich is only about one-half
that of a single substrate, even when care is taken to pit the
imbalance of the two substrates against one another. In either
case, the imbalance is not expected to be of any consequence for
180 rpm operation. Some measurements of the static droop of 1 mm
thick Glasflex substrates were made. On a 30 cm diameter disc
clamped to a diameter of 7.5 cm, the initial droop of the outer
edge is about 0.6 mm. After 16 hours of standing in that config-
uration (spindle axis vertical), the droop of the outer edge in-
creased to about 1 mm. Storage of the disc in the vertical position
(on edge) for two days and then returning it to the spindle indi-
cates no significant recovery during that time.

An optical displacement probe in conjunction with two differenti-
ation circuits is currently being used to measure the transverse
dynamic displacements, velocities, and accelerations. Data on
single-substrate plastic discs and air sandwich discs will be
available shortly.

Activity is now underway to determine the influence of artificial
aging on the mechanical and dimensional characteristics of
tellurium-coated Glasflex homopolymer samples. Initially the
time-temperature cycles will be similar to those presently used
in the investigation of the optical and sensitivity character-
istics of the same film/substrate combination. Specifically,
the elastic modulus, creep modulus, and linear dimensions of
coated tensile strips will be measured.

## 4.7     Life Testing of Tellurium and Bismuth Films

An investigation of the archival properties of tellurium and bismuth films has been initiated. The first results (see Appendix D) indicate that tellurium films do not degrade after exposure for 1500 hours at 90°C. Assuming an activation energy of 0.5 eV, this is equivalent to 8 1/2 years at room temperature. Previous experience with bismuth films has shown them to degrade fairly rapidly. Pinholes begin to form in bismuth films after aging at 100°C for 24 hours as shown in Figure 5. After one week at 100° C, the films of bismuth became completely transparent. It is not yet known how this will compare to aging under ambient conditions.
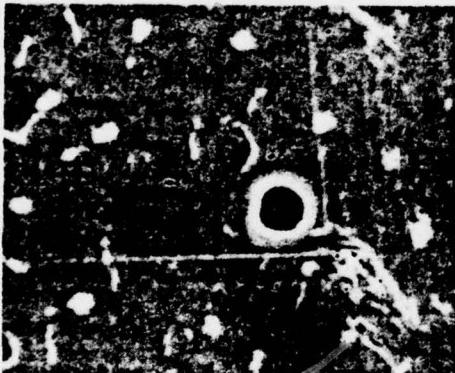


Figure 5: Pin hole in bismuth film.

The primary objective of the effort is to establish the projected lifespan of the recording materials by means of a series of controlled experiments done at various temperatures. This technique, known as temperature stress aging, is commonly used in industry to obtain some rough indications of projected life spans. The most convincing argument for its validity is the record of successful prediction of failure in the field. The technique will be used in this instance because of the need to generate 5-year life data in a 6-month program. The only apparent alternative is to do ambient aging over a 5-year life test program. Additional aging experiments will be conducted at room temperature as a reference for the results of the temperature stress aging.

While there are some reservations as to the ultimate validity of
temperature stress aging, PL believes this approach is a reason-
able starting point. Preliminary indications are that the degra-
dation of bismuth is by an oxidation process, possibly mediated
by some residual contaminants arising from the substrate side of
the film. Assuming that the chemical reactions are characterized
by a single activation energy $E_a$, then the reaction rate at any
given temperature T can be expressed in terms of the reaction
rate at a temperature $T_0$ by:

$$r(T)e^{\frac{E_a}{kT}} = r(T_0)e^{\frac{E_a}{kT_0}}$$

Thus, given $E_a$, one can calculate the degree of acceleration at
various temperatures compared to room temperature. Oxidation
processes for thin film degradation are typically thermally
activated with an activation energy between 0.5 eV to 1.0 eV.
Figure 6 shows the time acceleration factor versus activation
energy for the various test temperature. To obtain expected
archival life at 25°C, multiply life under test by the acdeler-
ation factor corresponding to the appropriate test temperature/
activation energy coordinate.

Samples will be subjected to different substrate treatments and
prepared and tested in parallel. They will be aged at the
specified temperatures, and their properties will be measured
at appropriate time intervals. In this time interval (three to
four months), a problem, if it does exist, should reveal itself.
The remainder of the program will be devoted to understanding
any degradation mechanism and attempting solutions or a more
extensive evaluation of the environmental conditions for
storage (such as humidity stress testing).
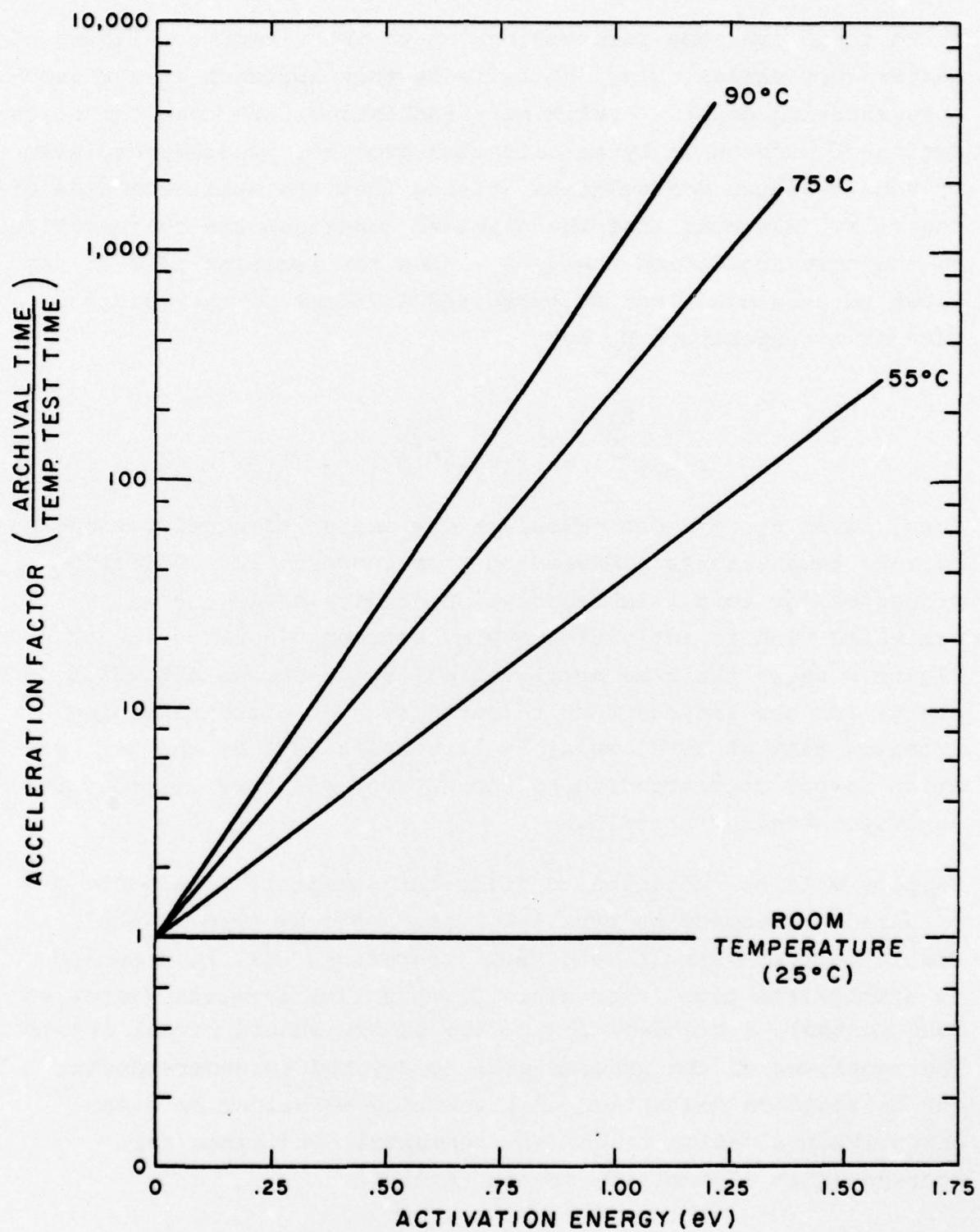
Figure 6

## 4.8 Digital Format, Codes and Error Correction

Another set of disc channel characterizations was obtained from NVP and studied. Theories of block code and convolutional code were studied. A triple-error convolutional code with interleaving of 256 bits was proposed by Magnavox for error correction. Final corrected error rates of $3.6 \times 10^{-10}$ are projected based on a raw error of $8 \times 10^{-5}$. A code efficiency of 66% and a maximum coder/decoder rate of 10 MHz are considered reasonable limitations for the first implementation. Further details of the proposed error correction technique is given in Appendix E.

Linkabit Corporation, San Diego, California, sells (as a standard product) a digital coder/decoder with triple-error correction and 256 bit interleaving. The final corrected error rate, $P_{out}$, is given as a function of the raw error rate $P_{in}$, by the following:

$$P_{out} = 1800 \, (P_{in})^4$$

This means that for the same $P_{in} = 8 \times 10^{-5}$, $P_{out} = 0.73 \times 10^{-13}$ (assuming no error bursts longer than 256 bits). Therefore, a desired $P_{out} \leq 10^{-9}$ will only require a $P_{in}$ of $0.86 \times 10^{-3}$. The maximum data rate of the Linkabit encoder/decoder is 0.5 Mbit/sec. Linkabit will study the possibility of increasing the data rate to 1.5 Mbit/sec or higher.

## 5. PLANS

a. Complete debugging PL recorder.

b. Record on an air sandwich disc.

c. Continue dynamic testing and characterization of tellurium discs.

d. Continue life testing of tellurium and bismuth films.

e. Continue work on subsystems to be refitted on back-up sled and turntable.

f. Finish first characterization of digital channel.

APPENDIX A

Techniques for Direct Measurement
of DRAW Optical Spots

by

D. A. Stanton

## TECHNIQUES FOR DIRECT MEASUREMENT OF DRAW OPTICAL SPOTS

D. A. Stanton

### INTRODUCTION

Standard techniques for observing, measuring, and aligning
the microscopic spots of light used in optical direct-read-
after-write (DRAW) schemes are too time-consuming and are
subject to error.  Techniques which could allow direct
observation and accurate measurement of these spots under
actual DRAW conditions are needed.  This report describes
a powerful tool which permits the observer to easily:

- Measure spot size accurately

- Prepare energy profiles of spots

- Optimize and position spots

- Observe tracks being written in real time

- Observe and evaluate tracking servos in operation

- Achieve all of the above in a condition of
  dynamic focus on the actual disc surface

A typical DRAW scheme is shown in Figure 1:
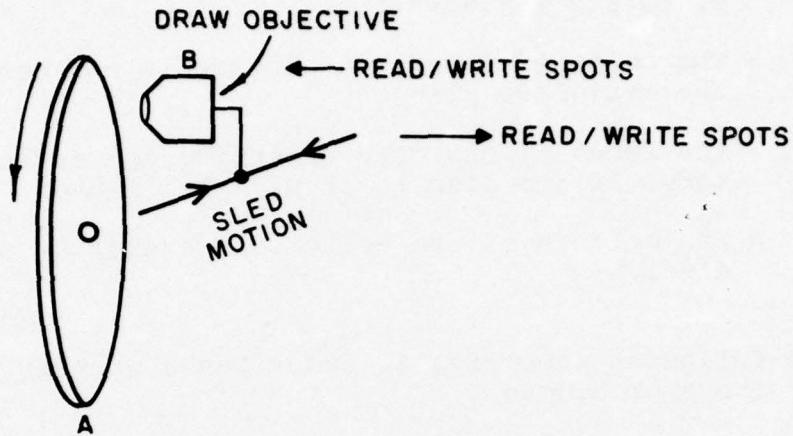


Figure 1

The substrate (A), on which is deposited a suitable material, rotates near a microscope objective (B) which is held in focus by a servo. Read and write spots are focused on the material, and the read/write process begins.

Crucial to the process is that all spots must be held in simultaneous focus at the material plane and that spot quality be maintained. Alignment of these spots is often accomplished by deactivating the auto focus servo, removing the disc, and placing a second projection objective (C) near the DRAW objective (B). The image thus produced is projected to (D) and used as the adjustment reference (see Fig. 2).
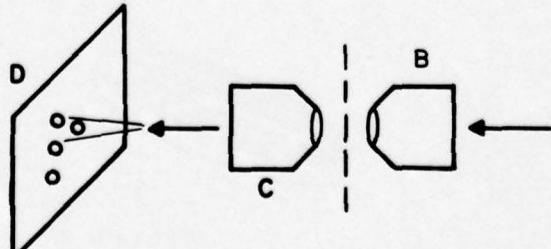


Figure 2

The limitations of this technique are:

- Positioning of the objectives is tedious, seldom repeatable, and sensitive to small errors in the x, Y, and Z planes.

- The point of focus coincidence is not necessarily the real disc plane.

- The focus of the DRAW objective is not held by the servo at the disc as it will be in use.

- The effects of the write beam cannot be seen (no disc).

The following (see Fig. 3) describes a working solution to the above problems:
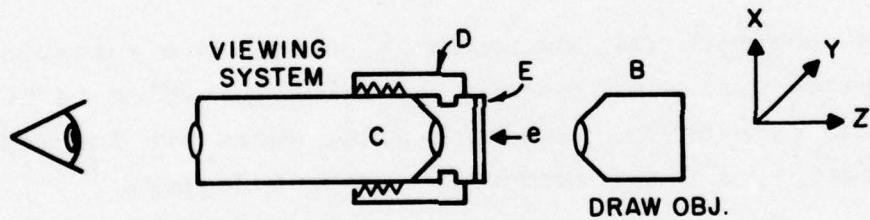
Figure 3

The objective (C) with a cap (D) is threaded onto (C) with a 100 pitch thread. Next, a cover slip (E) is fitted into a small depression in (D). This cover slip is prepared by depositing a few hundred angstroms of reflecting material on its surface (e) and carefully scratching the material, as shown in Figure 4.
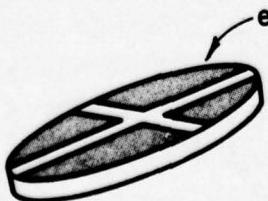
Figure 4

Having accomplished this, cap (D) is rotated until the scratch on the cover slip is in sharp focus. This cover slip has three basic functions:

- Provides a reflecting surface (E) onto which the DRAW objective (D) will focus automatically (Fig. 3)

- Ensures, via cap (D), that the viewing objective (C) is maintained in best focus and parallel to precisely the same surface (Fig. 3)

- Identifies and confirms the presence of the surface by means of the scratch

We have now configured a viewing system which allows stable focus on a well-defined plane, via a semi-transparent surface identified by a scratch. The viewing system is now placed in front of the DRAW objective and the auto focus system is activated.

Since the system will now maintain itself in alignment in the Z axis, the remaining conditions to be met are: image plane parallelism between (C) and (B), and X-Y adjustment. To achieve these requirements, the viewing system is held at the precise disc plane by simply piercing a glass master disc and mounting the system on it (Fig. 5).
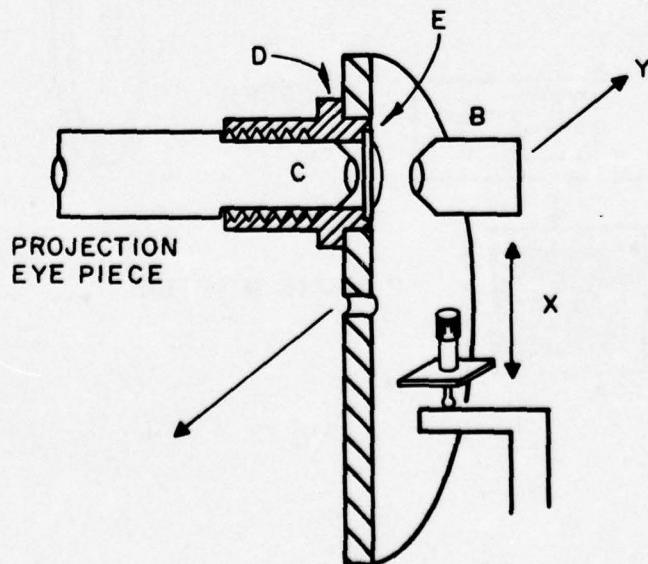


Figure 5

The (Y) adjustment is provided by normal objective traverse; the (X) adjustment is provided by a micrometer attached to the disc. We may now view of the spots as they appear during DRAW. Some caution must be observed when optimizing focus of spot groups. Each spot must be optimized at precisely the same location on the coated cover slip to minimize distortions in the viewing and DRAW objective; the X and Y adjustments permit this location.

## IMAGE ANALYSIS

Now that an accurate projected image can be achieved, the image must be analyzed. Of primary interest is: spot size ideally determined from an intensity profile of the spot in question, and a visual means of determining the spot position and overall quality. To achieve these goals, a television viewing system is employed (Fig. 6). A helpful technique for image analysis follows:



Figure 6

22
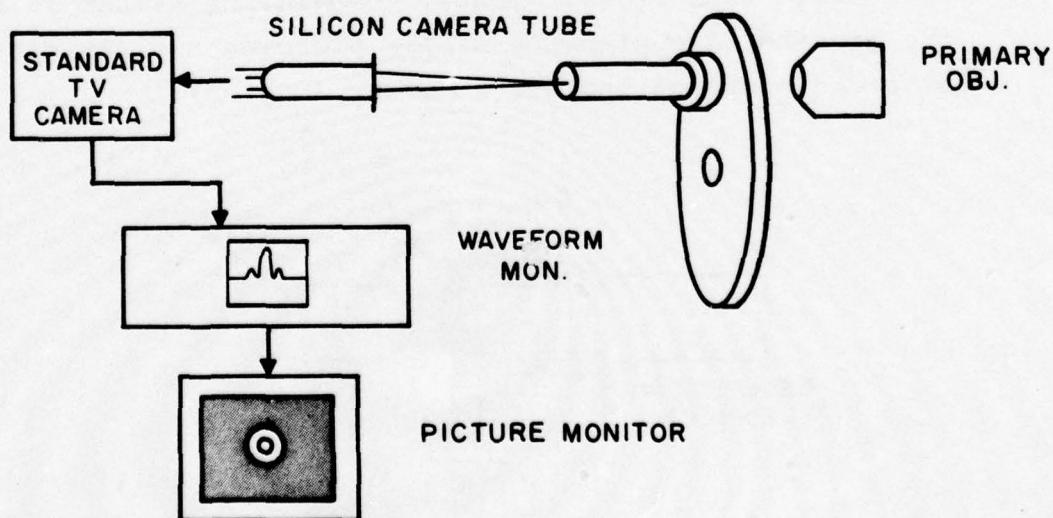
The spot to be analyzed is imaged on the semi-transparent layer of the cover slip and is projected directly onto a silicon TV pickup tube.  The resulting signal is fed to a standard video waveform monitor and to a picture monitor (Fig. 6).

The response of a typical silicon tube is shown in Fig. 7.
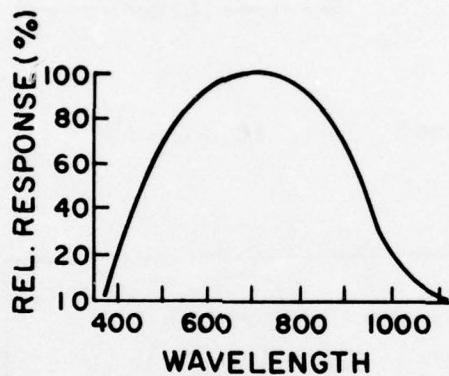


Figure 7

The silicon tube has adequate sensitivity over the wavelengths currently employed for DRAW activities and exhibits a linear intensity/signal characteristic.  The television waveform monitor, normally used for broadcast purposes, has several functions helpful in spot analysis.
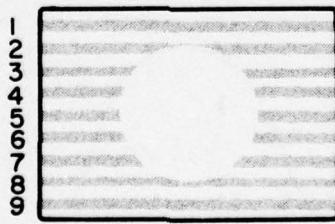


Figure 8

The white spot on a dark field (Fig. 8) may be presented in a variety of ways:

The 525 scan lines which comprise the picture may be presented in parade (Fig. 9):
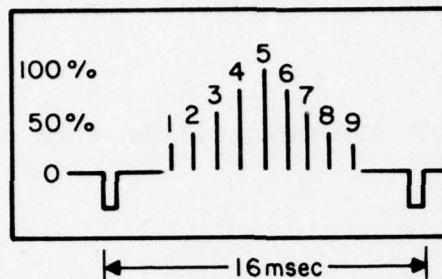


Figure 9

or superimposed (Fig. 10):
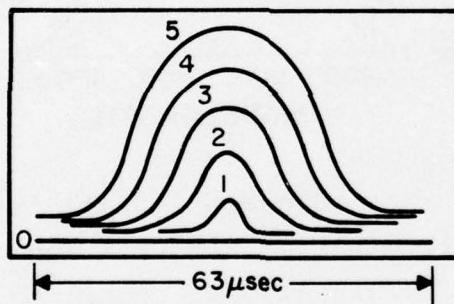


Figure 10

or presented singly (Fig. 11):
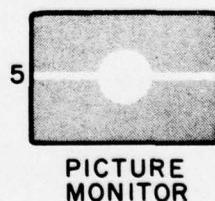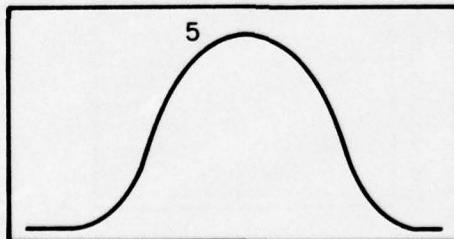


Figure 11

The line presented singly may be variably selected from any point on the picture and a marker or white intensified line will appear on the picture monitor at the point selected (Fig. 11).

24

All of the foregoing displays may be expanded 5x and 25x horizontally for better resolution of detail or smaller spots.  Since the horizontal scan velocity of the scanning TV line is constant and accurate, the horizontal time scale of the waveform monitor may be used as an accurate scale of distance.  A parade display calibration can be achieved which establishes one-tenth micron = 63 µs or one horizontal scan line.  Hence, in Fig. 9 the 50% intensity width of the spot is 0.4 µm.  Following are actual photographs of various micron size spots (see Figs. 12 thru 21).
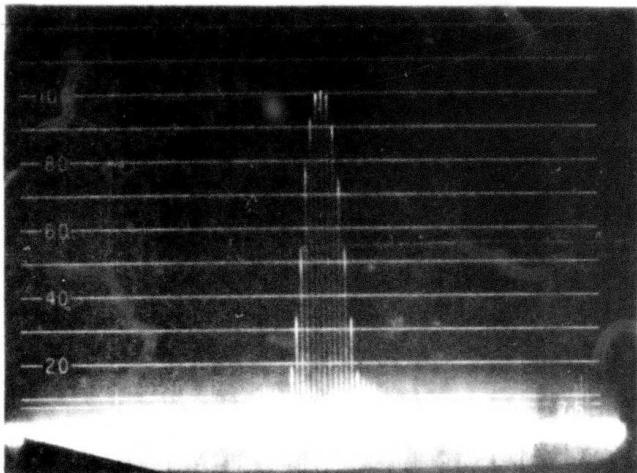
Figure 12: Blue write spot .1 µm/div horiz. .8 µm full width half maximum.
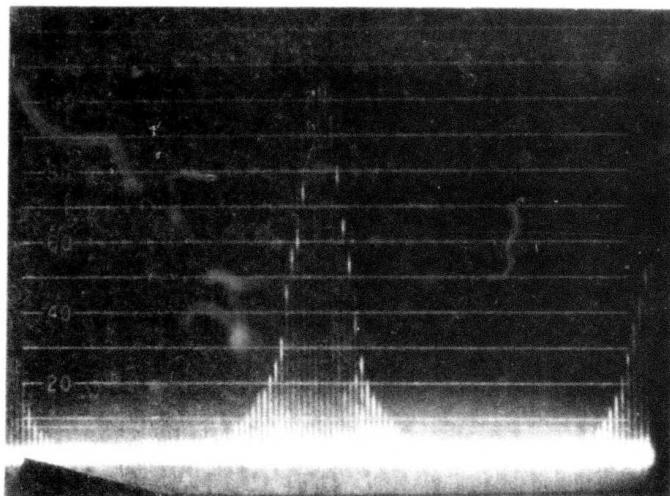


Figure 13: .1 µm/div, 1.2 µm full width half maximum.
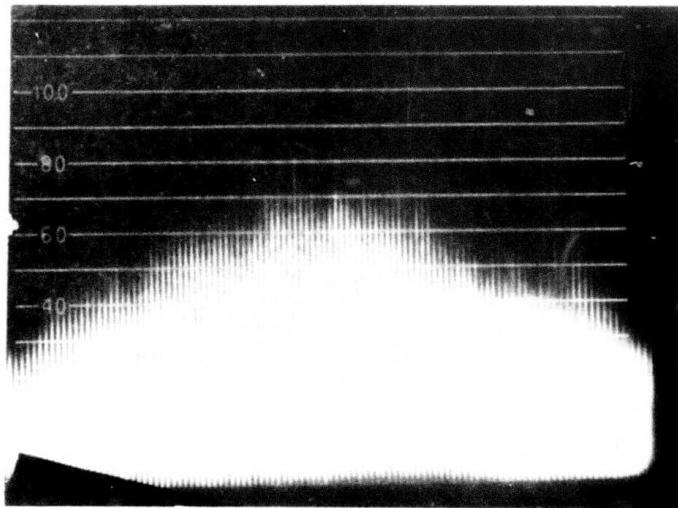


Figure 14: Red focus spot.

Figure 15: Picture monitor blue spot poorly focused.
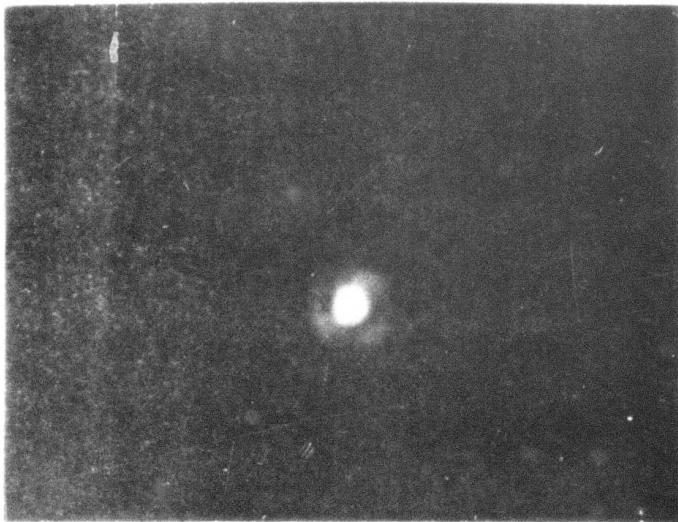


Figure 16: Picture monitor blue spot optimally focused. See Fig. 12 for waveform.
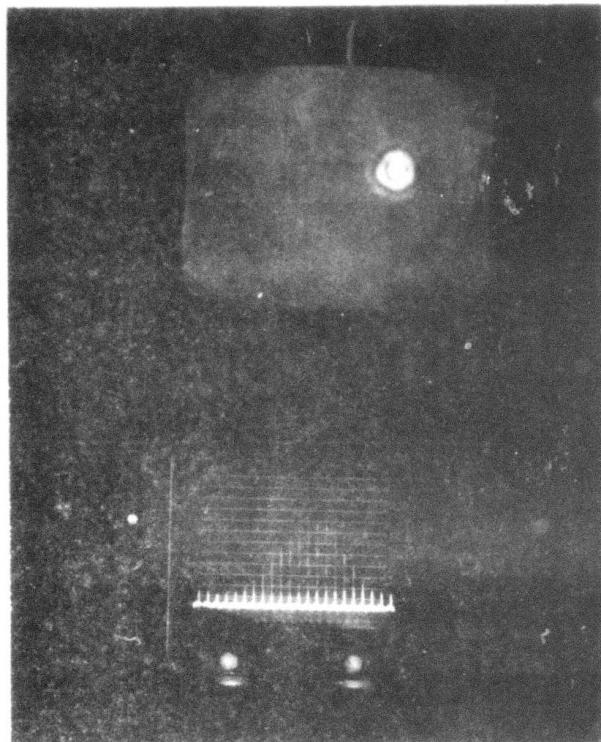
Picture monitor display
blue write spot.

Waveform monitor parade
display mag. 25X showing
center spot width of
1.1 µm FwHm.
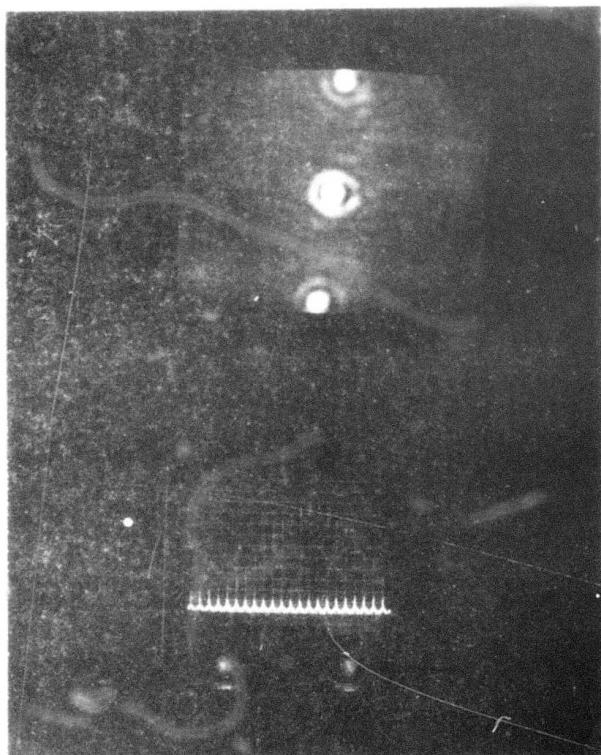
Figure 17



Picture monitor display
red read spot and radial
tracking spots.

Waveform monitor parade
display mag. 25X showing
high frequency spot
1.2 µm FwHm.

Figure 18

28
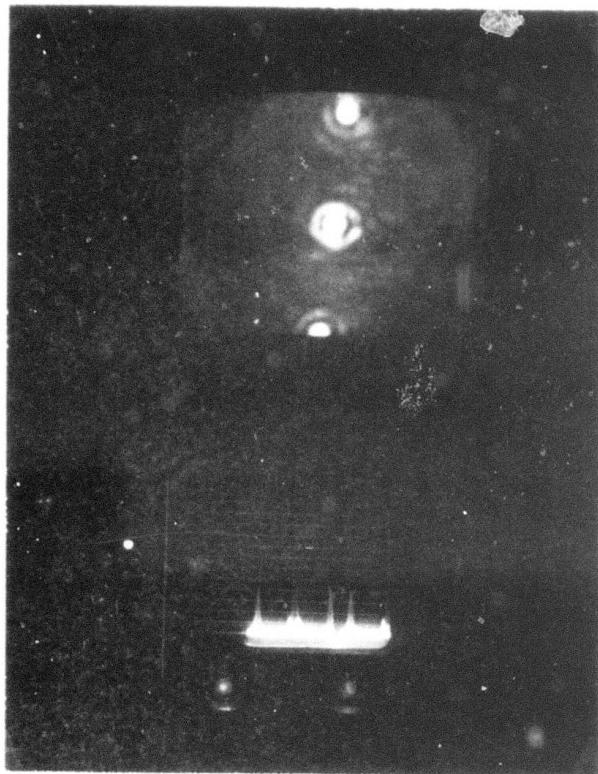
Picture of red read and radial tracking spots with resultant waveform monitor displays.
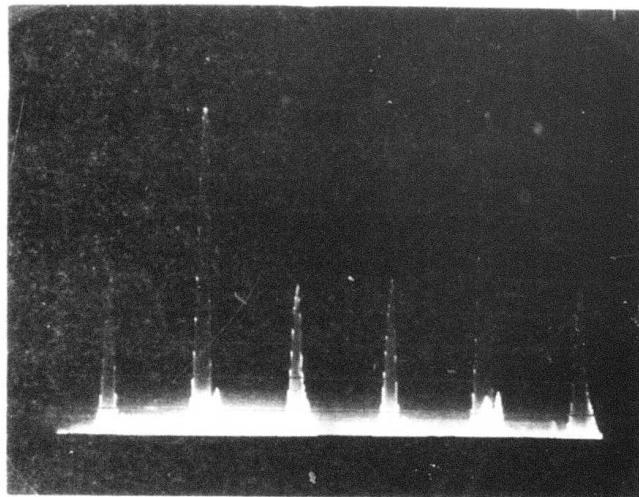


Two repetitions of spots. (see above photo).

Figure 19: Displays of a typical read and tracking 3 spot scheme.

SHEET 1 OF 2
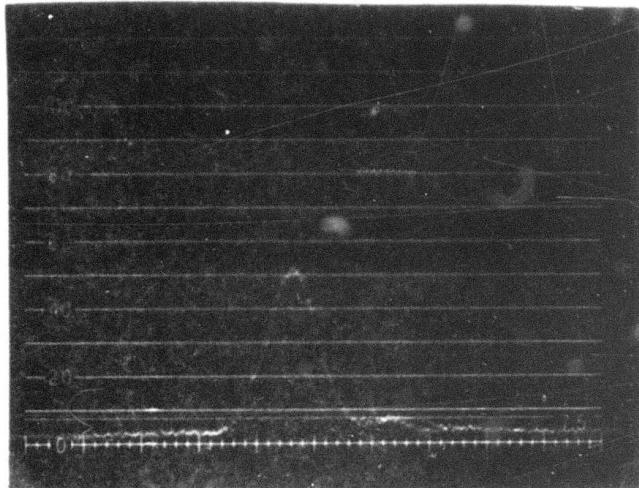
Top radial tracking spot.
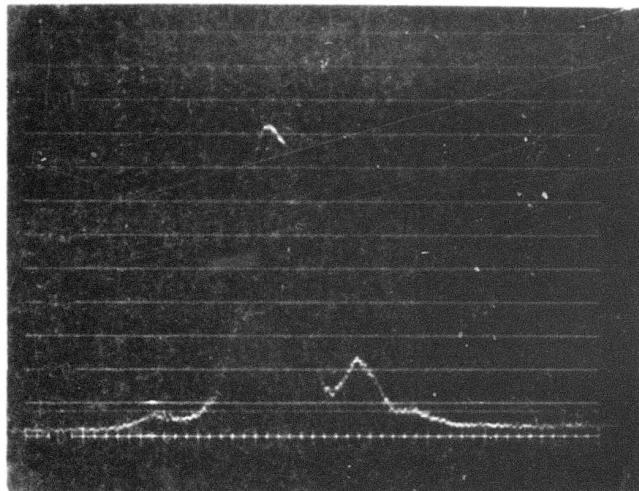
High frequency read spot.
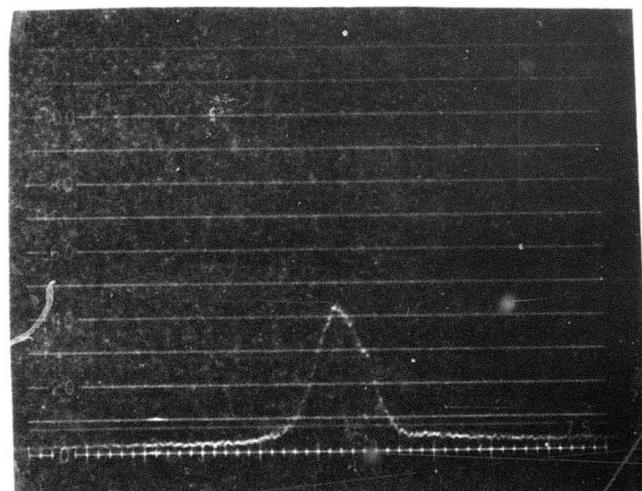
Bottom radial tracking spot.

Figure 19: Displays of a typical read and tracking 3 spot scheme.

SHEET 2 OF 2

30
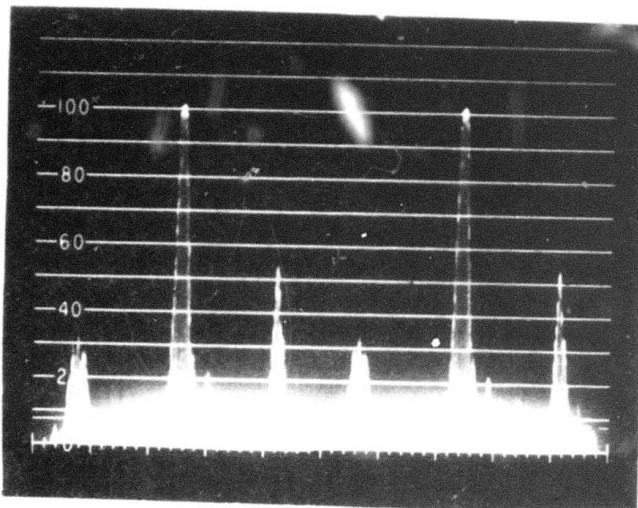
Figure 20: Red read spots showing poor radial tracking spot. Photo shows two repetitions of 3 spot cluster.
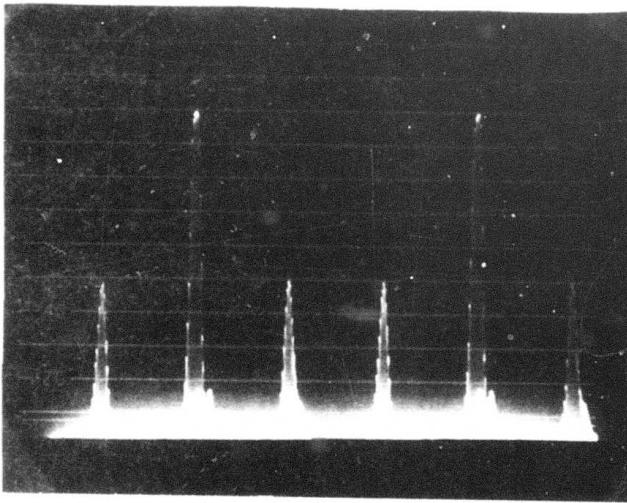


Figure 21: Red read spots corrected.

APPENDIX B


Spectral Absorption of Tellurium Films

by

D. Y. Lou

## SPECTRAL ABSORPTION OF TELLURIUM FILMS

The reflectance, transmittance and absorptance of thin films of
tellurium on polymethyl methacrylate substrates have been mea-
sured.   The results are summarized in the following tables.
The angle of incidence is 45° unless otherwise noted.

### TABLE I:   Reflectance

| Wavelength / Film Thickness | Argon 488 nm | He-Ne 633 nm | | GaAs 850 nm |
|---|---|---|---|---|
| 190 Å | 34% | 48% | 41% | 31% |
| 400 Å | 45% | 56% | 53% | 45% |
| 500 Å | 41% | 52% | 46% | 48% |
| 740 Å | 43% | 53% | 46% | 33% |
| | | | (90°) | |

### TABLE II:   Transmittance

| Wavelength / Film Thickness | Argon 488 nm | He-Ne 633 nm | | GaAs 850 nm |
|---|---|---|---|---|
| 190 Å | 13 % | 7.2% | 8.9 % | 31% |
| 400 Å | 2.0 % | 2.8% | 2.2 % | 13% |
| 500 Å | 0.84% | 1.4% | 1.1 % | 10% |
| 740 Å | 0.36% | 0.54% | 0.24% | 10% |
| | | | (90°) | |

### TABLE III:   Absorptance

| Wavelength / Film Thickness | Argon 488 nm | He-Ne 633 nm | | GaAs 850 nm |
|---|---|---|---|---|
| 190 Å | 53% | 45% | 50% | 38% |
| 400 Å | 53% | 41% | 45% | 42% |
| 500 Å | 58% | 46% | 53% | 42% |
| 740 Å | 57% | 48% | 54% | 57% |
| | | | (90°) | |

Assuming that the laser micromachining process is a purely
thermal process, the only dependence of the sensitivity on
wavelength should be that due to changes in absorption.  Sen-
sitivities of the tellurium films at 633 nm and at 850 nm
should therefore be within 25% of that measured at 488 nm.

# APPENDIX C

## Some Thoughts on the Choice of Optimum Lens
## for Laser Recording on a Moving Substrate

by

D. Y. Lou

## SOME THOUGHTS ON THE CHOICE OF OPTIMUM LENS
## FOR LASER RECORDING ON A MOVING SUBSTRATE

In a real time optical recording process which allows readout immediately after write in, the size of the information pit is controlled solely by the power density distribution in the writing laser beam. This contrasts with non-real time processes where development can be used to control pit size. It is therefore much more important in real time recording to have the proper optical design so as to achieve the optimum pit structure. In this note we shall present some preliminary considerations, based on a simple model of the laser recording process, regarding the proper choices of the writing objective lens spot size.

Figure 1 shows the model we have taken for the laser recording process. The absorption of laser irradiation produces an energy density distribution $E(x,y)$ in the recording medium. A pit is formed wherever $E(x,y)$ is greater than a critical energy density $E_c$. The pit boundary $(x_h, y_h)$ can therefore be defined by the equation

$$E(x_h, y_h) = E_c \tag{1}$$

The model is valid only when heat diffusion can be neglected.

### Case I - Static Writing

The laser beam is stationary with respect to the substrate. The power density distribution at the focal point of the lens changes depending on the aperture and overfill conditions. However, in general, one can approximate the distribution by a gaussian function with a certain beam radius $r_o$ and peak power density $P(o)$. The special case for the overfilled weak focussing lens is considered in Appendix C1 of this Appendix.

Thus we shall limit our considerations to the power density distribution

$$P(r) = P(o) \exp(-r^2/r_o^2) \tag{2}$$

After an exposure duration $\tau$, the total energy absorbed by the film is

$$E_t = \int_{r=0}^{\infty} \tau \, P(r) \, 2\pi r \, dr$$

$$= \pi r_o^2 \, \tau \, P(o) \tag{3}$$

The pit radius $r_h$ versus laser energy $E_t$ is given by the relationship

$$E_t = \pi r_o^2 \, E_c \, \exp(r_h^2/r_o^2) \tag{4}$$

and minimum energy is required to form a pit of radius $r_h$ when

$$\frac{dE_t}{dr_o} = o \tag{5}$$

$$r_o = r_h$$

This result has been obtained by Maydan.

## Case II – Dynamic Writing

Consider now the case when the laser beam is moving at a velocity $v$ in the x direction with respect to the substrate. The laser beam is turned on during the time interval $(-\frac{\tau}{2}, \frac{\tau}{2})$ and the gaussian peak passes $x = o$ at $t = o$. We shall approximate the power density distribution at the focal plane with an astigmatic gaussian function of the appropriate peak power density $P(o)$ and beam length $x_o$, width $y_o$. The special case for a circular beam with $x_o = y_o = r_o$ is considered in Appendix C2. Thus

$$E(x,y) = \int_{-\frac{\tau}{2}}^{\frac{\tau}{2}} P(o) \, \exp(-y^2/y_o^2)$$

$$\exp\left[-\left(\frac{x-vt}{x_o}\right)^2\right] dt$$

$$= \frac{E_t}{\pi x_o y_o} \, \exp(-y^2/y_o^2)$$

$$\cdot \frac{\sqrt{\pi}}{4} \left(\frac{2x_o}{v\tau}\right) \left\{ \operatorname{erf}\left(\frac{x + v\tau/2}{x_o}\right) - \operatorname{erf}\left(\frac{x - v\tau/2}{x_o}\right) \right\} \tag{6}$$

The pit contour $(x_h, y_h)$ satisfies the equation

$$\frac{E_t}{\pi x_o y_o} \exp\left(\frac{-y_h^2}{y_o^2}\right) \frac{\sqrt{\pi}}{4} \left(\frac{2x_o}{v\tau}\right)$$

$$\cdot \left[ \text{erf}\left(\frac{x_h + v\tau/2}{x_o}\right) - \text{erf}\left(\frac{x_h - v\tau/2}{x_o}\right) \right] = E_c \tag{7}$$

Figure 2 shows some typical pit contours. The pits produced are elongated in the x direction. The choice of the optimum beam radii $x_o, y_o$ depends on the pit characteristic we wish to optimize. In the following discussion we shall examine the proper choices of $x_o$, $y_o$ as a function of the pit characteristics desired. We shall show that, in general, to optimize the characteristics in the x direction, it is desirable to have $x_o$ as small as possible, while to optimize the characteristics in the y direction, an optimum $y_o$ exists, where $y_o$ is larger then the half pit width. We shall also show that operations with $y_o$ smaller than the half pit width which can lead to gross instabilities in the writing characteristics. From these considerations we shall then arrive at the choice numerical aperture for the writing objective lens.

(a)  The pit length $2x_s$ is defined by

$$x_s = x_h \big)_{y_h = 0} \tag{8}$$

$$\frac{E_t}{\pi x_o y_o} \frac{\sqrt{\pi}}{4} \left(\frac{2x_o}{v\tau}\right) \left\{ \text{erf}\left(\frac{x_s + v\tau/2}{x_o}\right) - \text{erf}\left(\frac{x_s - v\tau/2}{x_o}\right) \right\} = E_c \tag{9}$$

For any $y_o$, minimum energy is required to form a pit of any arbitrary length $2x_s$ when

$$\frac{\partial E_t}{\partial x_o}\bigg)_{x_h = x_s, \ y_h = 0} = 0 \tag{10}$$

$$\frac{x_s + v\tau/2}{x_o} \exp\left[ -\left(\frac{x_s + v\tau/2}{x_o}\right)^2 \right]$$

$$= \frac{x_s - v\tau/2}{x_o} \exp\left[ -\left(\frac{x_s - v\tau/2}{x_o}\right)^2 \right]$$

$$x_o = 0 \tag{11}$$

Figure 3 shows the amount of energy $E_t$ required to form pits of length $2x_s = v\tau$ for various values of $v\tau$ and $x_o$. For any given $x_o$, $x_s$ and $v\tau$, the amount of energy required is linearly proportional to $y_o$.

(b) The noise in the signal is related to the uncertainty in the pit edge, which can be qualitatively measured by the quantity $\delta = \left( \dfrac{x_s}{E_c} \dfrac{\partial E(x,y)}{\partial x} \right)^{-1}_{x=x_s,\ y=o}$. Choosing $x_s = v\tau/2$, Eq. (6) yields

$$\frac{1}{\delta} = \frac{\frac{1}{2} \frac{v\tau}{x_o} \{1 - \exp[-(\frac{v\tau}{x_o})^2]\}}{\operatorname{erf}(\frac{v\tau}{x_o})} \tag{12}$$

In typical recording applications, $v\tau > x_o$ and increasing $v\tau$ decreases $\delta$. $\delta$ is minimum when $x_o = o$. Increasing $y_o$ does not affect $\delta$. Figure 4 plots this equation.

(c) The pit width $2y_s$ is defined by

$$y_s = y_h)_{x_h = o} \tag{13}$$

$$\frac{E_t}{\pi x_o y_o} \exp\left(-\ y_s^2/y_o^2\right) \frac{\sqrt{\pi}}{2} \left(\frac{2x_o}{v\tau}\right) \operatorname{erf}\left(\frac{v\tau}{2x_o}\right) = E_c \tag{14}$$

For proper readout and radial tracking, it would be desirable to have a certain minimum pit width. Minimum energy is required to produce a given pit width $y_s$ when

$$\frac{\partial E_t}{\partial y_o} )_{x_h = o,\ y_h = y_s} = o \tag{15}$$

$$y_o = \sqrt{2} y_s \tag{16}$$

At optimum the energy required to form a pit of width $y_s$ is then

$$\frac{E_{min}}{E_s} = \frac{4}{\sqrt{\pi e}} \frac{x_o}{y_o} \frac{v\tau/2x_o}{\operatorname{erf}(v\tau/2x_o)} \tag{17}$$

41

where $E_s = e\pi y_s^2 E_c$ is the energy required to form a pit of radius $y_s$ in the static case. This is shown in Fig. 5. For $v\tau > 2x_o$, $E_{min}$ is linear in $v\tau$. Reducing $x_o$ decreases $E_{min}$ by a small amount. At $x_o = y_o = \sqrt{2}y_s$, $v\tau = 4y_s = 2.8 x_o$, $E_{min} \approx 2.0 E_s$.

Operating away from the optimum, we have, from Eq. (14)

$$\frac{E_t}{E_s} = \frac{x_o}{y_s} \, (\frac{y_o}{y_s}) \, \exp \, (\frac{y_s^2}{y_o^2} - 1)$$

$$\cdot \left[ \frac{\frac{2}{\sqrt{\pi}} \, \frac{v\tau}{2x_o}}{\mathrm{erf} \, (\frac{v\tau}{2x_o})} \right] \tag{18}$$

This situation is plotted in Fig. 6. Operating away from optimum in the direction of a fine focus beam can be extremely costly in energy. Thus, using a beam of $x_o = y_o = 0.5y_s = 0.35 \, (y_s\sqrt{2})$, $v\tau = 4y_s = 8x_o$, Eq. (18) gives us $E_t = 60 \, E_s$.

(d)  The instability in pit width with respect to variations in write laser energy is measured by

$$\eta = \frac{\partial y_s/y_s}{\partial E_t/E_t} = \frac{y_o^2}{2y_s^2} \tag{19}$$

The most stable pit widths are obtained when $y_o = 0$.

(e)  The variation in write laser energy required to produce a pit of width $y_s$ with respect to variations in beam diameter $y_o$ is given by

$$\varepsilon = \frac{\partial E_t/E_t}{\partial y_o/y_o} = 1 - \frac{2y_s^2}{y_o^2} \tag{20}$$

This is shown in Figure 7. The instability is minimum when,

42

$$y_O = \sqrt{2} y_s \tag{22}$$

Operations away from optimum in the direction of a fine focus beam can lead to great instabilities in the writing laser power required depending on the beam diameter obtained out of the objective lens. Using a beam of $x_O = y_O = 0.5\ y_s = 0.35\ (y_s \sqrt{2})$, at $v\tau = 4y_s = 8\ x_O$, Eq. (20) gives us

$$\frac{dE_t}{E_t} = 7\ \frac{dy_O}{y_O}$$

(f)  The symmetry in pit length is given by

$$\sigma = \frac{2x_s}{v\tau} - 1 \tag{22}$$

Equation (7) gives us

$$2 \exp (-y_s{}^2/y_O{}^2)\ \ \text{erf}\ \ (\frac{v\tau}{2x_O})$$

$$= \ \text{erf}\ (\frac{x_s + v\tau/2}{x_O})\ - \text{erf}\ (\frac{x_s - v\tau/2}{x_O}) \tag{23}$$

From Eq. (23) we can obtain a plot of $\sigma$ versus $v\tau$ and $y_s$.  This is done in Fig. 7.  The best symmetry is obtained when

$$\sigma = 0$$

$$\frac{y_O{}^2}{y_s{}^2} = \frac{1}{\ln \dfrac{2\ \text{erf}\ (\frac{v\tau}{2x_O})}{\text{erf}\ (\frac{v\tau}{x_O})}}$$

For $v\tau > 2x_o$, this yields

$$y_o \approx 1.2y_s$$

The use of a finely focused beam also leads to degradation in pit symmetry.

Thus, for example, Eq. (23) shows that at $x_o = y_o = 0.5y_s$, $v\tau = 4y_s = 8x_o$, we find $x_s = 5.4x_o$, $\frac{2x_s}{v\tau} = 1.35$. The pits are much longer than the interpit spacings. If we adjust the power level so that $x_s = v\tau$, $y_s = 0.8y_o = 0.1v\tau$ becomes an extremely narrow pit. This situation is clearly shown in Figure 2.

To summarize, the considerations presented above suggests strongly that, subject to the validity of our model for the laser recording process, the use of a tightly focused laser beam obtained from an overfilled high numerical aperture objective lens is not desirable for direct read after write optical recording. Since the recording process is not coupled in the directions parallel to (x) and perpendicular to (y) the direction of substrate motion, the optimum writing beam is an astigmatic beam, tightly focused in the x direction. but defocused in the y direction so that the beam diameter $2y_o$ in the y direction is approximately 1.4 times the pit width $2y_s$ desired.
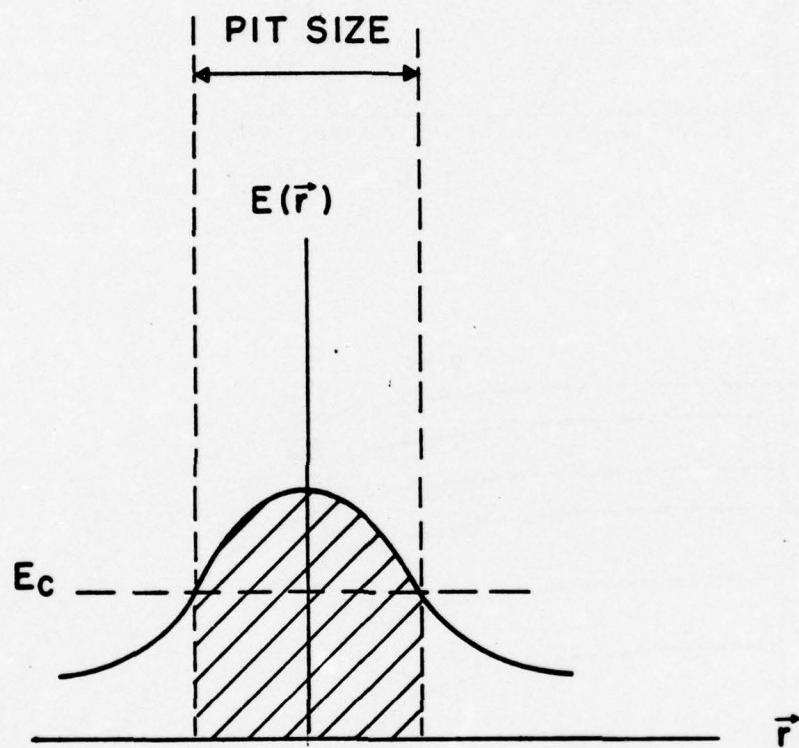
Figure 1: Model for laser recording process. Pit size is determined by a critical energy density $E_c$.
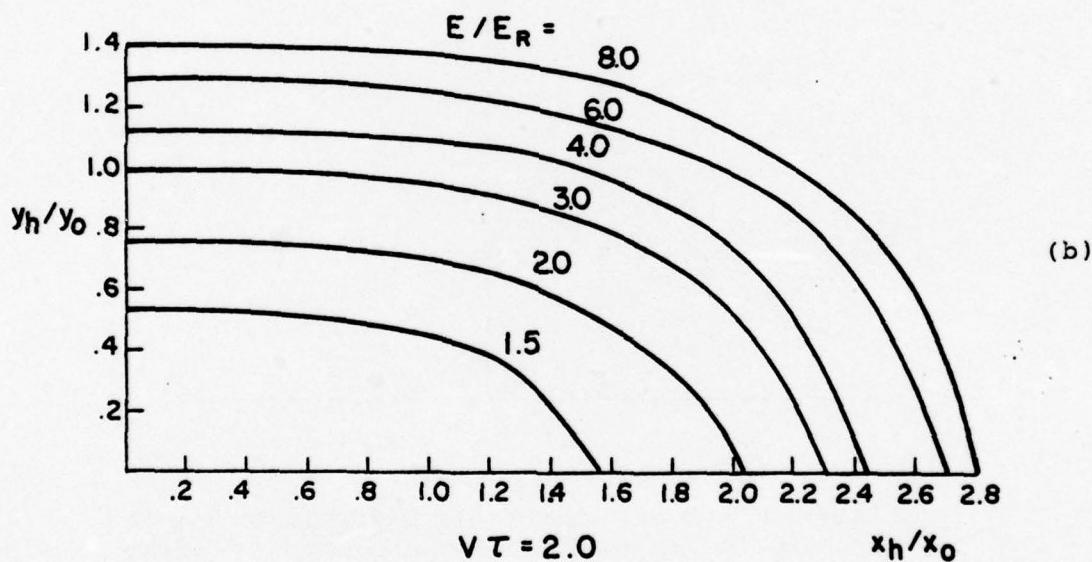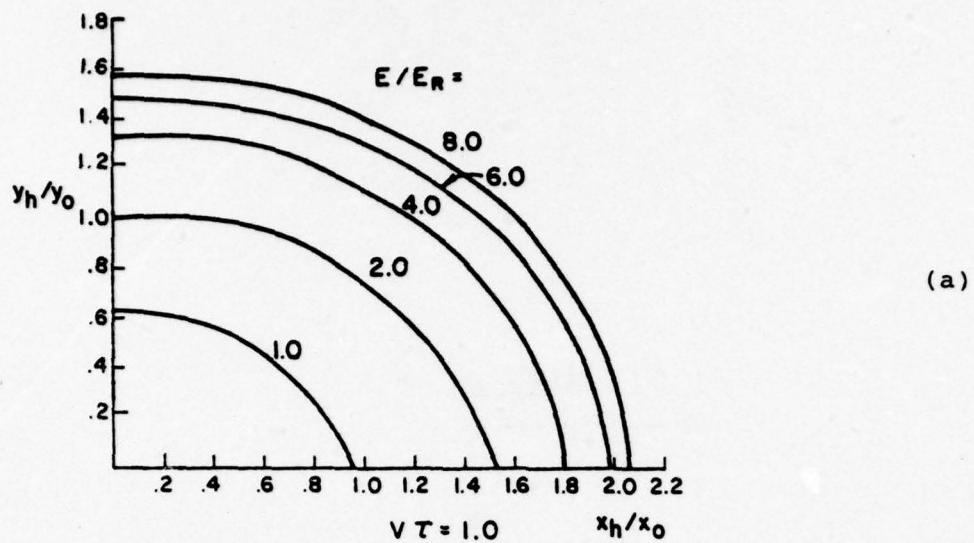
Figure 2: Equi-energetic (isothermal) contours in the film material for various substrate velocities.

(Sheet 1 of 2)
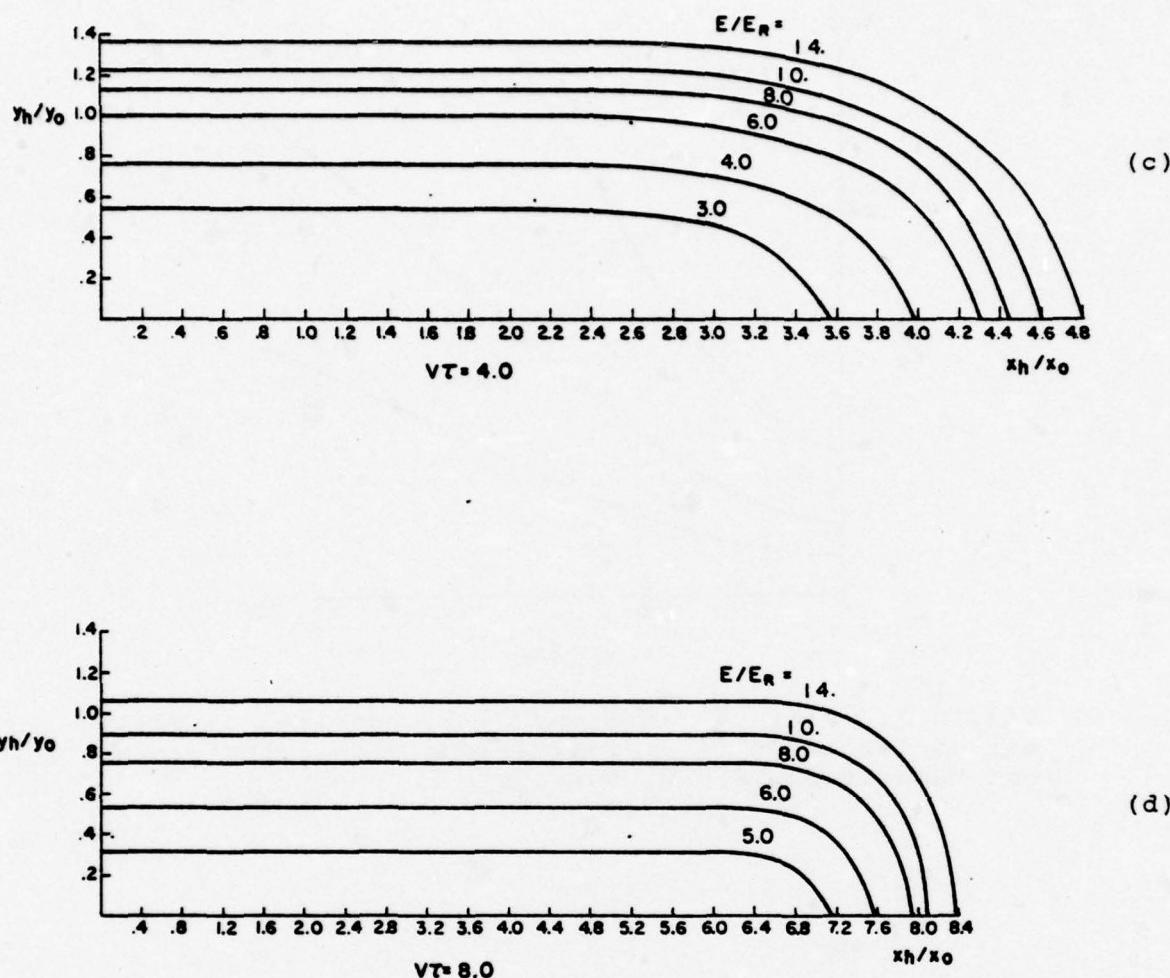
46

Figure 2:  Equi-energetic (isothermal) contours in
the film material for various substrate velocities.

(Sheet 2 of 2)

47
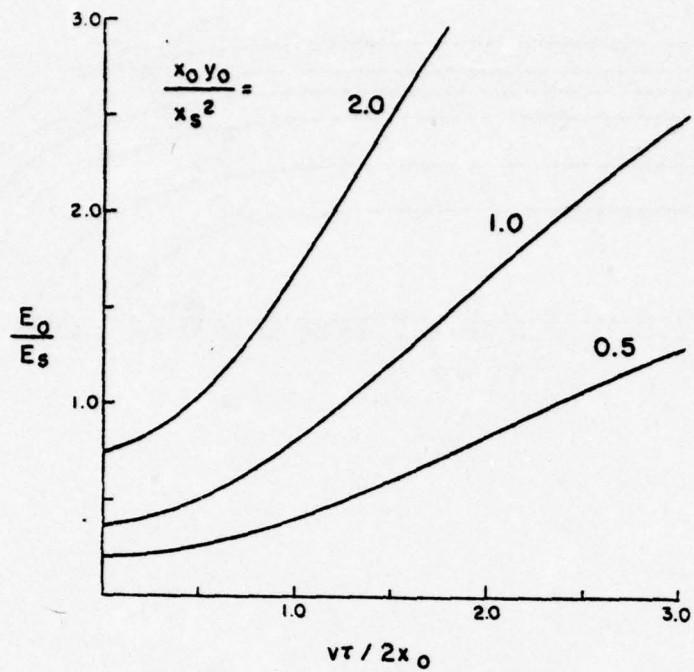
Figure 3: Plot of laser energy $E_t$ required to write pit of length $2x_s = v\tau$ for various beam diameters $x_o$, $y_o$ and velocities $v\tau$. $E_s = e\pi x_s^2 E_c$.
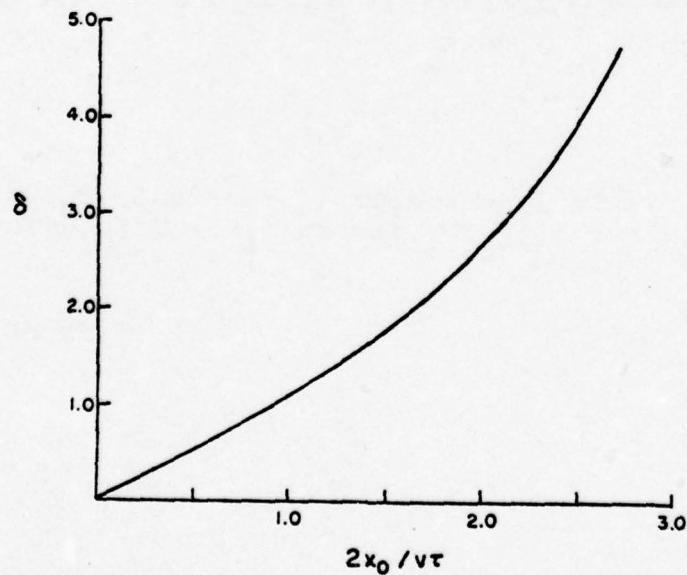


Figure 4: Plot of edge noise $\delta = 1/\dfrac{x_s}{E_c} \dfrac{\partial E}{\partial x} )_{x=x_s, y=0}$ vs. beam length $x_o$.
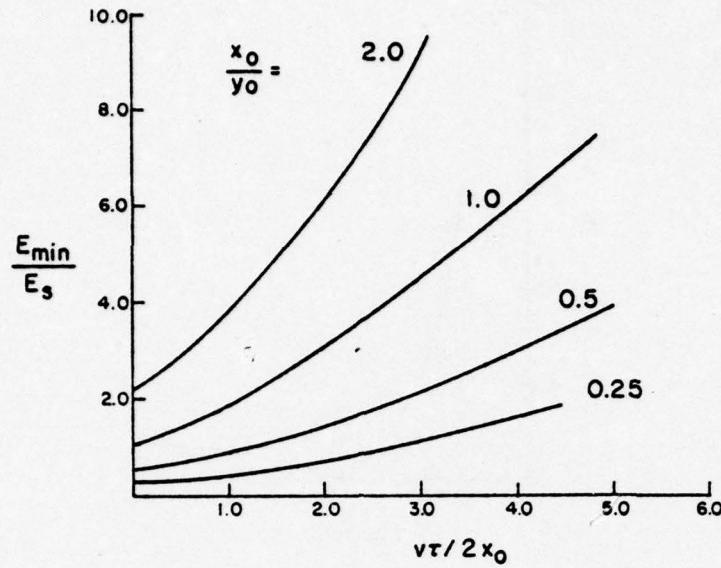
Figure 5: Plot of optimum energy $E_{min}$ required to write a pit of given width $y_s$ as a function of velocity $E_s = e\pi \, y_s^2 E_c$.
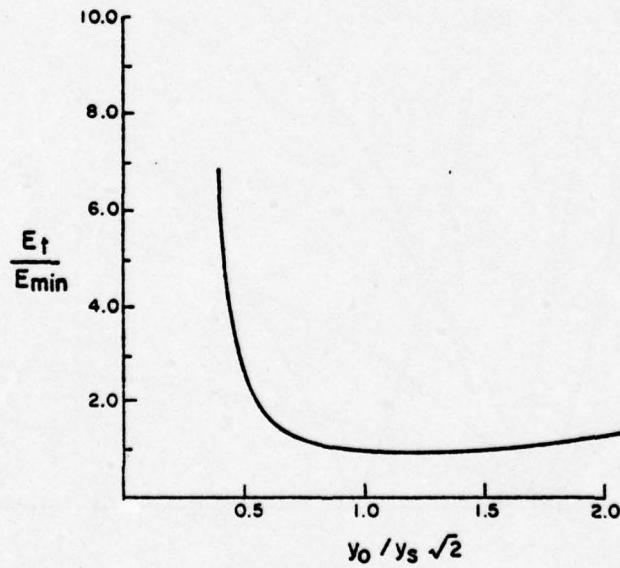


Figure 6: Plot of laser energy $E_t$ required to write pits of width $y_s$ as a function of beam width $y_o$.
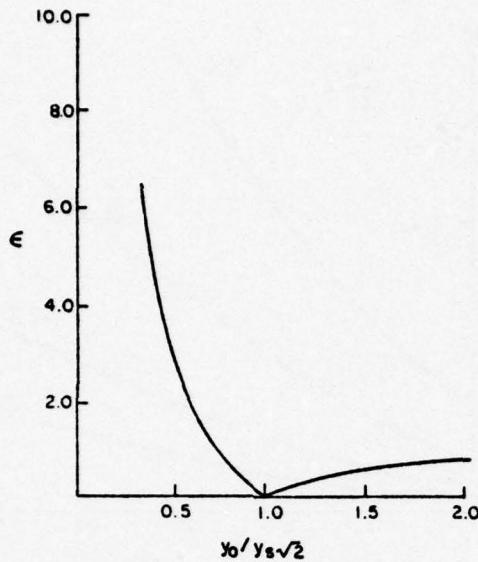
Figure 7:  Plot of the instability in writing laser energy with respect to beam diameter $\varepsilon = \dfrac{\partial E_t/E_t}{\partial y_o/y_o}$ as a a function of laser beam width $y_o$.
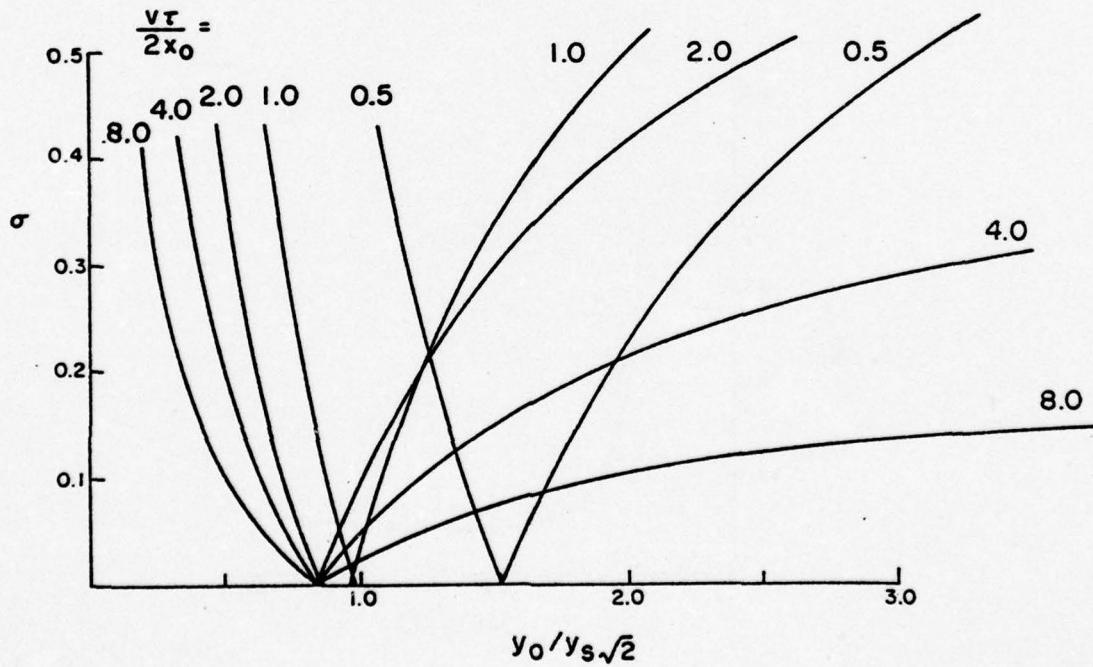


Figure 8:  Plot of pit symmetry $\sigma = \dfrac{2x_s}{v\tau} - 1$ as a function of laser beam width $y_o$.

<div align="center">

### APPENDIX C1

</div>

When a weak focusing lens is grossly overfilled the power density distribution is given by the classical Airy formula.

$$P(r) = P(o) \left[\frac{2J_1(r/\rho)}{r/\rho}\right]^2 \tag{A1}$$

where

$$\rho = \frac{\lambda}{2\pi} \left(\frac{1}{N.A.}\right) \tag{A2}$$

Because of overfilling, this represents only a small fraction of the total power incident on the lens.

For static writing, after an exposure duration $\tau$, the total energy absorbed by the film is

$$E_t = \int_{r=o}^{\infty} \tau \, P(r) \, 2\pi r dr$$

$$= 2\pi\rho^2 \, P(o) \, \tau \int_{\eta=o}^{\infty} \left[\frac{2J_1(\eta)}{\eta}\right]^2 \eta d\eta$$

$$= 4\pi\rho^2 \, \tau \, P(o) \tag{A3}$$

and Eq. (4) can be written as

$$E_t = \frac{\pi r_h^2 \, E_c}{[J_1(r_h/\rho)]^2} \tag{A4}$$

For a given lens and writing wavelength, $\rho$ is fixed, and minimum energy is required to produce a pit of radius $r_h$ when $J_1(r_h/\rho)$ is maximum, i.e., when

$$r_h/\rho = \frac{2\pi(N.A.)r_h}{\lambda} = 1.8 \tag{A5}$$

$$J_1(r_h/\rho) = 0.58$$

The optimum lens numerical aperture for producing 0.80 μm diameter pits with 488 nm radiation is N.A. = 0.29, with an Airy disc diameter of 2.0 μm. A lens with N.A. = 0.75, Airy disc diameter of 0.80 μm, is optimum for producing pits of diameter $2r_h = 0.31$ μm.

The gaussian and Airy distribution are compared in Figure A1. Here the two distributions are normalized so that the optimum beam diameters and total energies are equal.

$$r_o = 1.8\rho = \frac{0.29\lambda}{N.A.} \tag{A6}$$

$$P(o)_{gaussian} = \frac{E_t}{\pi r_o^2}$$

$$= \left(\frac{2}{1.8}\right)^2 \frac{E}{4\pi\rho^2} = 1.2\, P(o)_{Airy} \tag{A7}$$

Thus, even in the worst case of gross overfilling, it is reasonable to approximate with a gaussian beam, provided one chooses the parameters with formulas similar to (A6) and (A7).
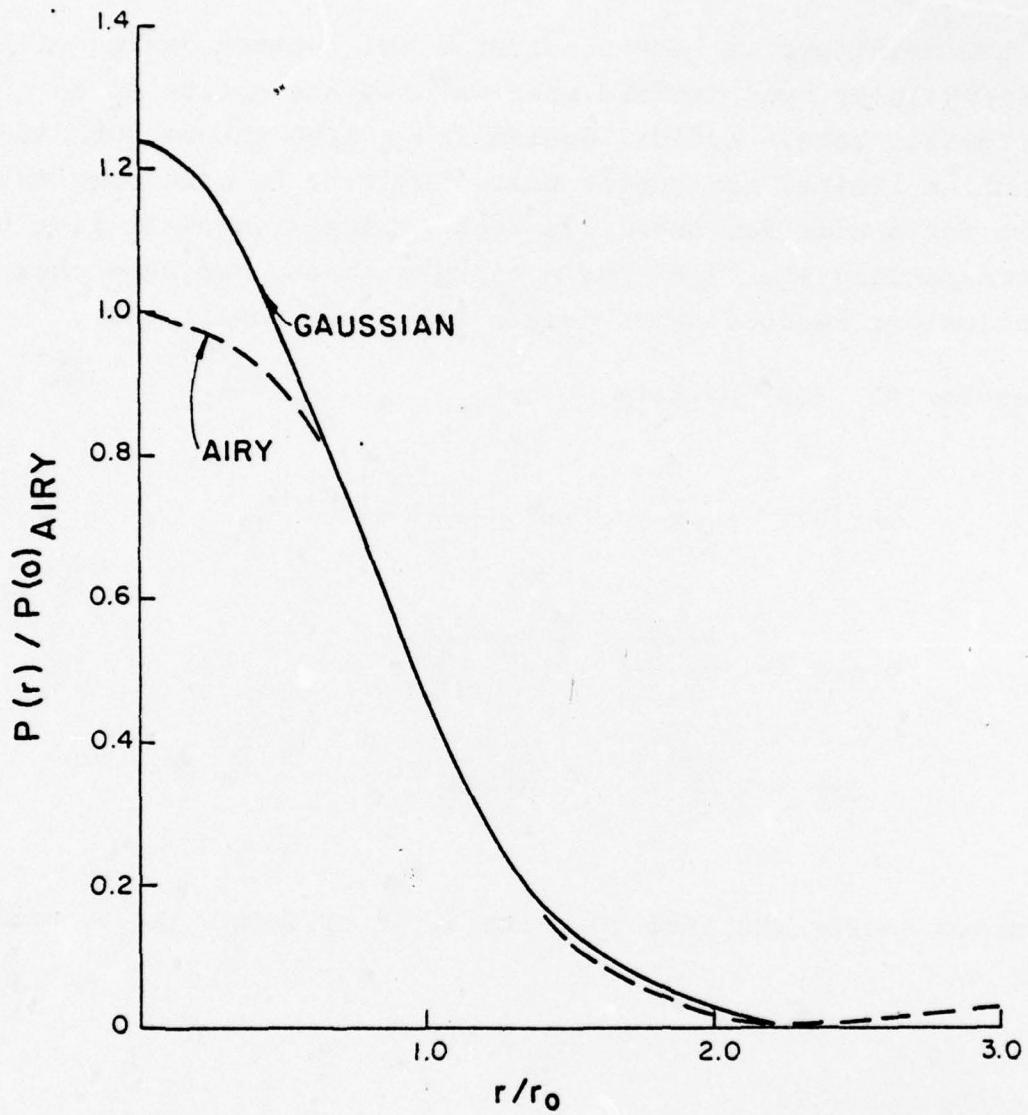
Figure A1: Comparison of Airy and Gaussian distribution $r_o = \frac{1.8\rho\lambda}{2\pi(NA)}$ for Airy distribution. $r_o$ = power to the 1/e point for gaussian distribution.

### APPENDIX C2

In the main text we have considered the optimum design of the writing laser spot profile when we have the option of an astigmatic beam. Optical design for a high throughput diffraction limited astigmatic beam, however, is more complex than that for a circular beam. In this appendix we shall list the corresponding equations for a circular beam, and show that the conclusions reached above remain relatively unaffected.

Thus for Eq. (10) we have

$$\frac{\sqrt{\pi}}{2} \left[ \text{erf}\ (\frac{x_s + \frac{v\tau}{2}}{r_o}) - \text{erf}\ (\frac{x_s - \frac{v\tau}{2}}{r_o}) \right]$$

$$= \exp\ [-\ (\frac{x_h - \frac{v\tau}{2}}{r_o})^2\ ]\ (\frac{x_h - \frac{v\tau}{2}}{r_o})$$

$$-\ \exp\ [-(\frac{x_h + \frac{v\tau}{2}}{r_o})^2\ ]\ (\frac{x_h + \frac{v\tau}{2}}{r_o}) \tag{B1}$$

Minimum energy required to write a pit of length $2x_s$ occurs at

$$r_o = 0 \tag{B2}$$

Eq. (12) becomes

$$\frac{1}{\delta} = \frac{\frac{1}{2} \frac{v\tau}{r_o} \left\{ 1 - \exp[-\ (\frac{v\tau}{r_o})^2] \right\}}{\text{erf}\ (\frac{v\tau}{r_o})} \tag{B3}$$

Minimum pit edge noise still occurs at

$$r_o = 0 \tag{B4}$$

Eq. (16) becomes

$$\frac{r_o^2}{2y_s^2} = \frac{1}{\dfrac{\dfrac{2}{\sqrt{\pi}}\dfrac{v\tau}{2r_o}}{\mathrm{erf}(\frac{v\tau}{2r_o})\exp[(\frac{v\tau}{2r_o})^2]} + 1} \tag{B5}$$

This is plotted in Fig. (B1). Equation (B5) reduces to Eq. (16) for $v\tau > 4r_o$.

Equation (17) is replaced by

$$\frac{E_{min}}{E_s} = \frac{\dfrac{4}{\sqrt{\pi e}}(\frac{v\tau}{2r_o})\exp\left[\dfrac{\dfrac{1}{\sqrt{\pi}}\dfrac{v\tau}{2r_o}}{\mathrm{erf}\frac{v\tau}{(2r_o)}\exp[(\frac{v\tau}{2r_o})^2]}\right]}{\dfrac{2}{\sqrt{\pi}}(\frac{v\tau}{2r_o})\exp[-(\frac{v\tau}{2r_o})^2] + \mathrm{erf}(\frac{v\tau}{2r_o})} \tag{B6}$$

This is shown in Fig. (B2). For $v\tau > 4r_o$, the write laser energy required is still linearly proportional to $v\tau$.

Equation (18) is replaced by

$$\frac{E_t}{E_s} = \frac{r_o^2}{y_s^2}\exp(\frac{y_s^2}{r_o^2} - 1)\frac{\dfrac{2}{\sqrt{\pi}}\dfrac{v\tau}{2r_o}}{\mathrm{erf}(\frac{v\tau}{2r_o})} \tag{B7}$$

This is shown in Fig. (B3). Operations away from optimum in the direction of a tightly focussed beam are still quite costly in energy.

The instability in pit widths with respect to variations in write laser energy is given by

$$\eta = \frac{r_o^2}{2y_s^2} \tag{B8}$$

The most stable pit widths are obtained when $r_o = 0$.

The variation in write laser energy required to produce a pit of width $y_s$ with respect to variations in beam diameter $r_o$ is given by

$$\varepsilon = 1 - \frac{2y_s^2}{r_o^2} + \frac{\frac{v\tau}{2r_o} \exp\left[-\left(\frac{v\tau}{2r_o}\right)^2\right]}{\operatorname{erf}\left(\frac{v\tau}{2r_o}\right)} \tag{B9}$$

This is shown in Fig. (B4).

Similarly Eq. (7) is now given by

$$2 \exp\left(-\frac{y_s^2}{r_o^2}\right) \operatorname{erf}\left(\frac{v\tau}{2r_o}\right)$$

$$= \operatorname{erf}\left(\frac{x_s + v\tau/2}{r_o}\right) - \operatorname{erf}\left(\frac{x_s - v\tau/2}{r_o}\right) \tag{B10}$$

and $\sigma = 0$ when

$$\frac{r_o^2}{y_s^2} = \frac{1}{\ln\dfrac{2\operatorname{erf}\left(\frac{v\tau}{2r_o}\right)}{\operatorname{erf}\left(\frac{v\tau}{r_o}\right)}} \tag{B11}$$
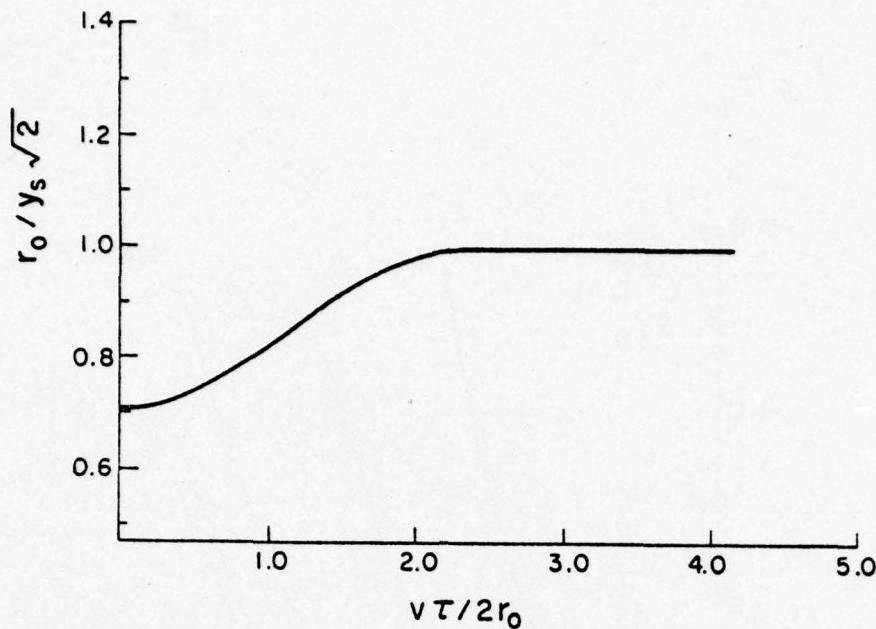
Figure B1: Plot of optimum beam diameter for laser machining as a function of substrate velocity.
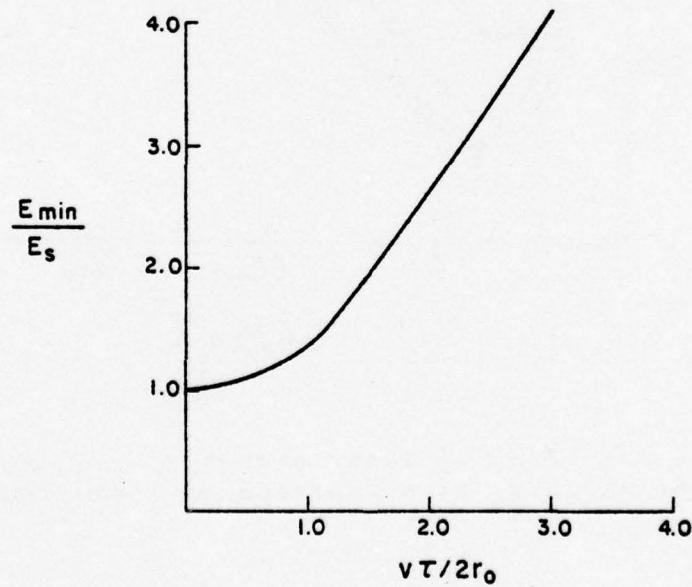


Figure B2: Plot of the minimum energy $E_{min}$ required to machine a pit of width $y_s$ as a function of substrate velocity.
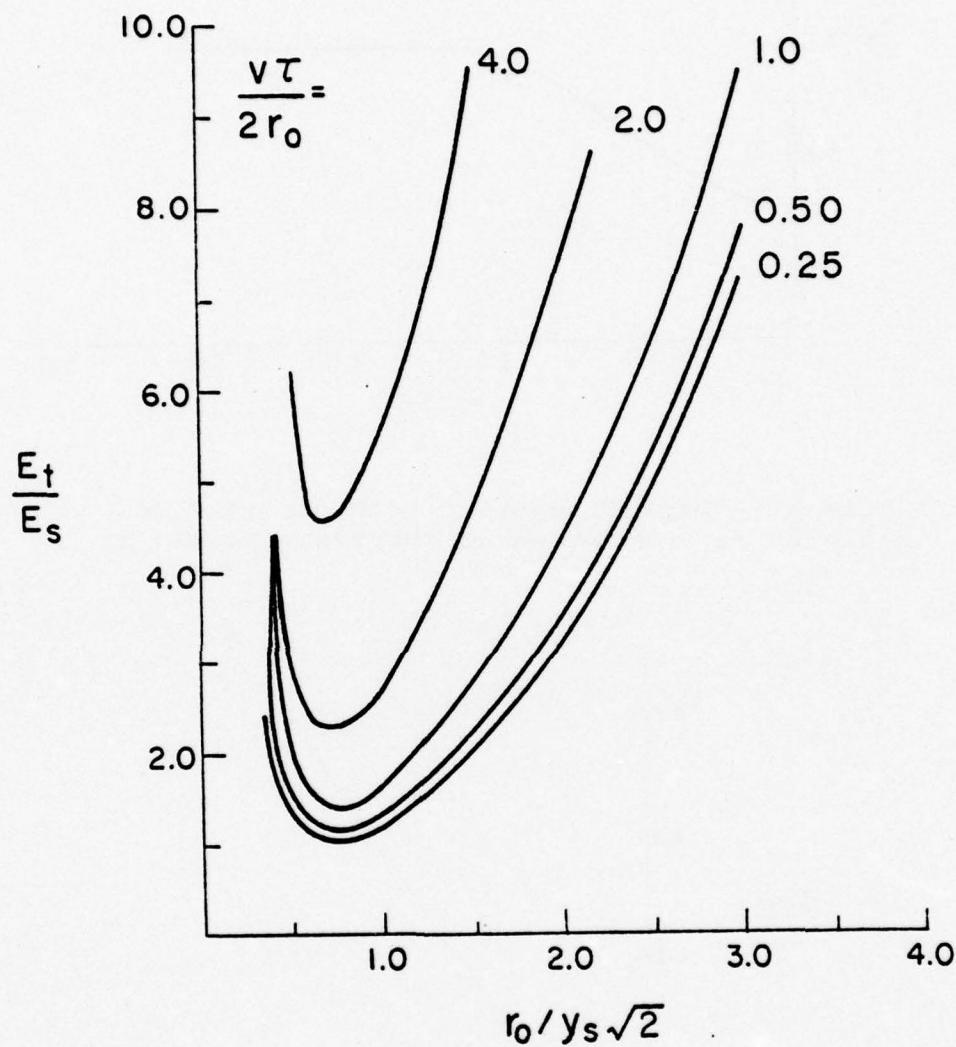
Figure B3: Plot of laser energy $E_t$ required to write pits of width $y_s$ as a function of beam diameter $2r_o$.

APPENDIX D


Archival Testing of DRAW Films

by

A. Milch

## ARCHIVAL TESTING OF DRAW FILMS

A total of 20 evaporations were made to study the archival properties of tellurium and bismuth films. Eight test pieces were produced per evaporation for a total of 160 samples. The substrates tested included PMMA Glasflex homopolymer, PMMA Glasflex copolymer, PMMA from MCA, and glass. 300 Å tellurium and bismuth films were deposited normally on the four substrates. Characteristics under study are reflecton, transmission, and hole machining sensitivity to He-Ne and Argon lasers. The samples are aged at 25°C, 55°C, 75°C and 90°C. Maximum aging time is 2500 hours as of September 30.

All quantitative measurements taken thusfar show, with the single exception of thickness, very wide variations -- as much as a factor of two in some cases. Hence, individual or sparsely distributed measurements should be held in some reserve pending the accumulation of more densely packed statistics. To date the results are as follows:

1. <u>Sensitivity for machining 1 μm holes.</u>

   - Tellurium ~300 mJ/$cm^2$. Very little change with age, temperature, substrate (Glasflex homopolymer and copolymer only) up to ~2000 hours life (see graph 1).

   - Bismuth ~600 to 800 mJ/$cm^2$ independent of age (up to ~300 hours life), temperature, and (Glasflex) substrate (data very sparce, see graph 2).

2. <u>Transmission/reflection/absorption.</u>

   - Te on Glasflex homopolymer and copolymer shows little change up to over 2000 hours aging at all test temperatures (see graphs 3, 4, 5, 6, 7, 8).

   - Bi on the same substrates shows a steady drift after some tens of hours in the direction of diminishing reflection and increasing transmission at all temperatures.

3. <u>Thickness</u>.

Standard film dimensions are 18 mm diameter x 300 Å thick except where otherwise noted. Film thickness was measured on glass substrate gravimetrically (assuming bulk density) and via the Sloan Deposit Rate Monitor. Generally the two results agreed to within 5%.

Holes were machined by means of argon ($\lambda$ = 4880 Å) laser using powers ranging from ≃2 to 30 mW, modulated to produce 750 nsec pulses at repetition times of 100 µsec the resultant holes were between 0.2 µm and > 7 µm diameter. The holes were photographically recorded at 2000X magnification and visual inspection under a 10X graticule calibrated to ± 0.2 mm. Using this technique hole sizes from ≤ 1.0 µm to 8 µm were determined as closely as possible.

GRAPH 1

GRAPH 2

ROOM TEMP. AGING OF Te on HOMOPOLYMER PLASTIC

GRAPH 3

GRAPH 4

GRAPH 5

ROOM TEMP. AGING OF
Te on HOMOPOLYMER
PLASTIC

GRAPH 6

E 10 o
E 12 △
E 24 □

55°C AGING OF Tø
ON HOMOPOLYMER
PLASTIC

HOURS ——▶

GRAPH 7

ABSORPTION (%)

90°C AGING OF Te
ON HOMOPOLYMER
PLASTIC
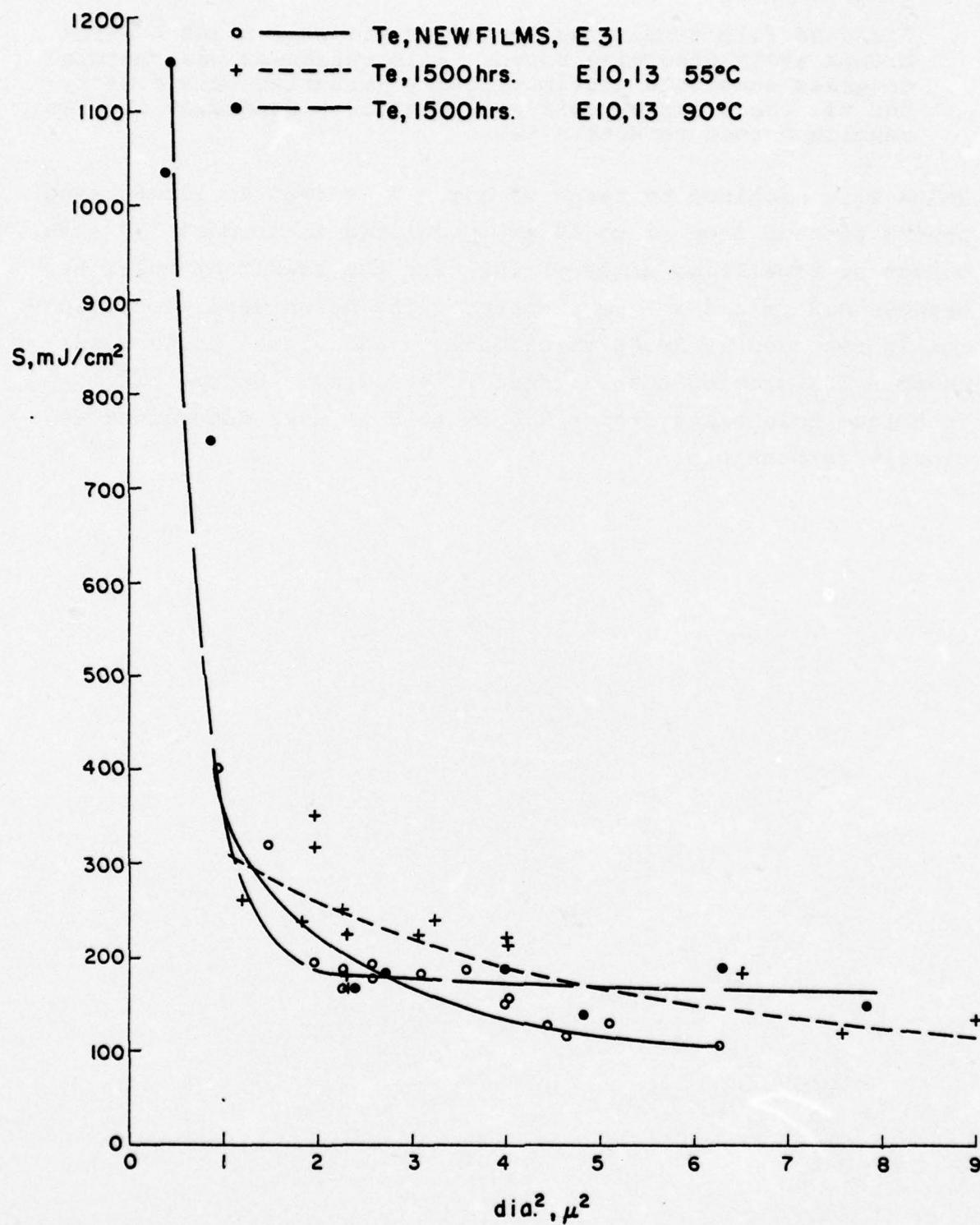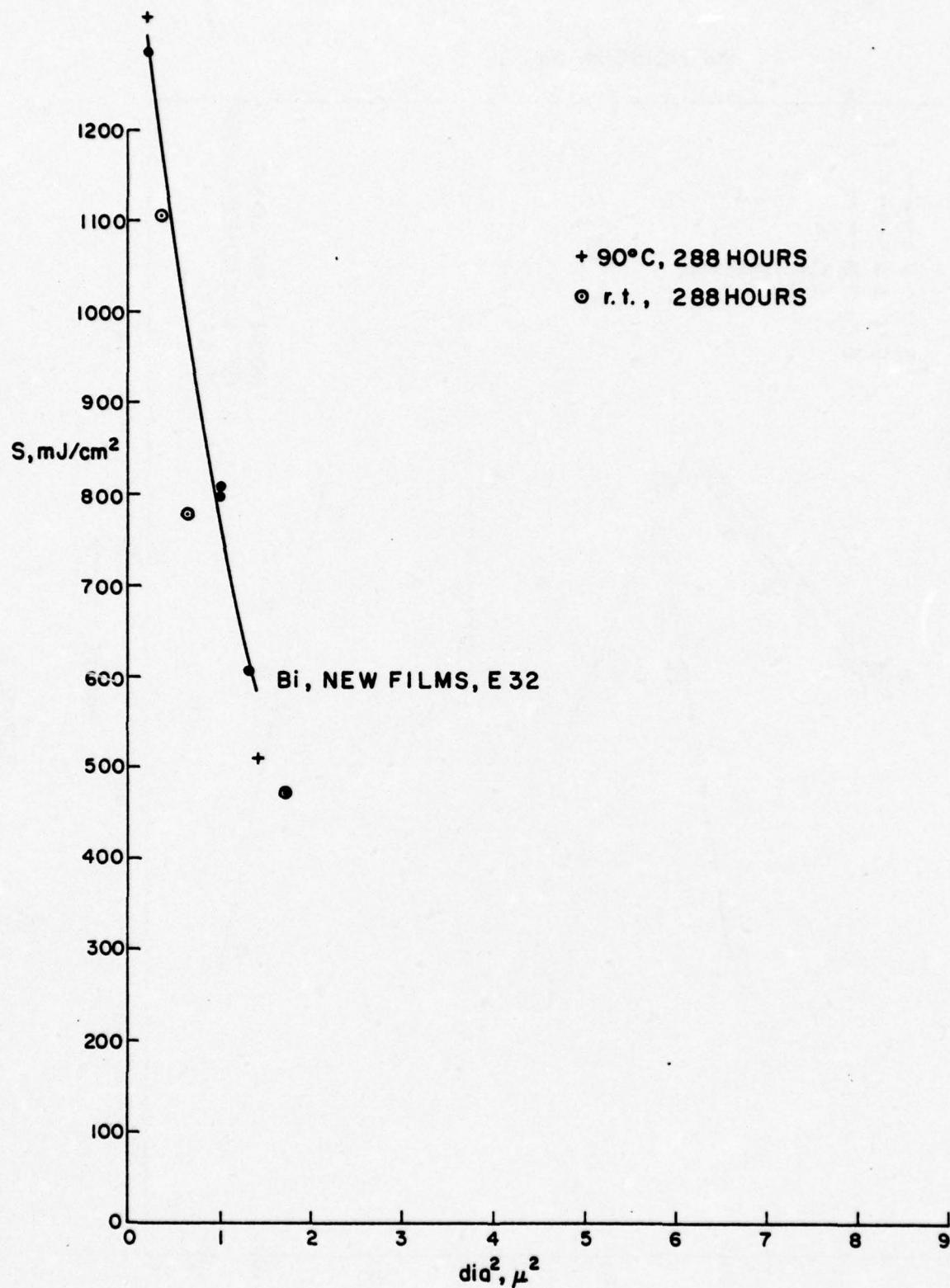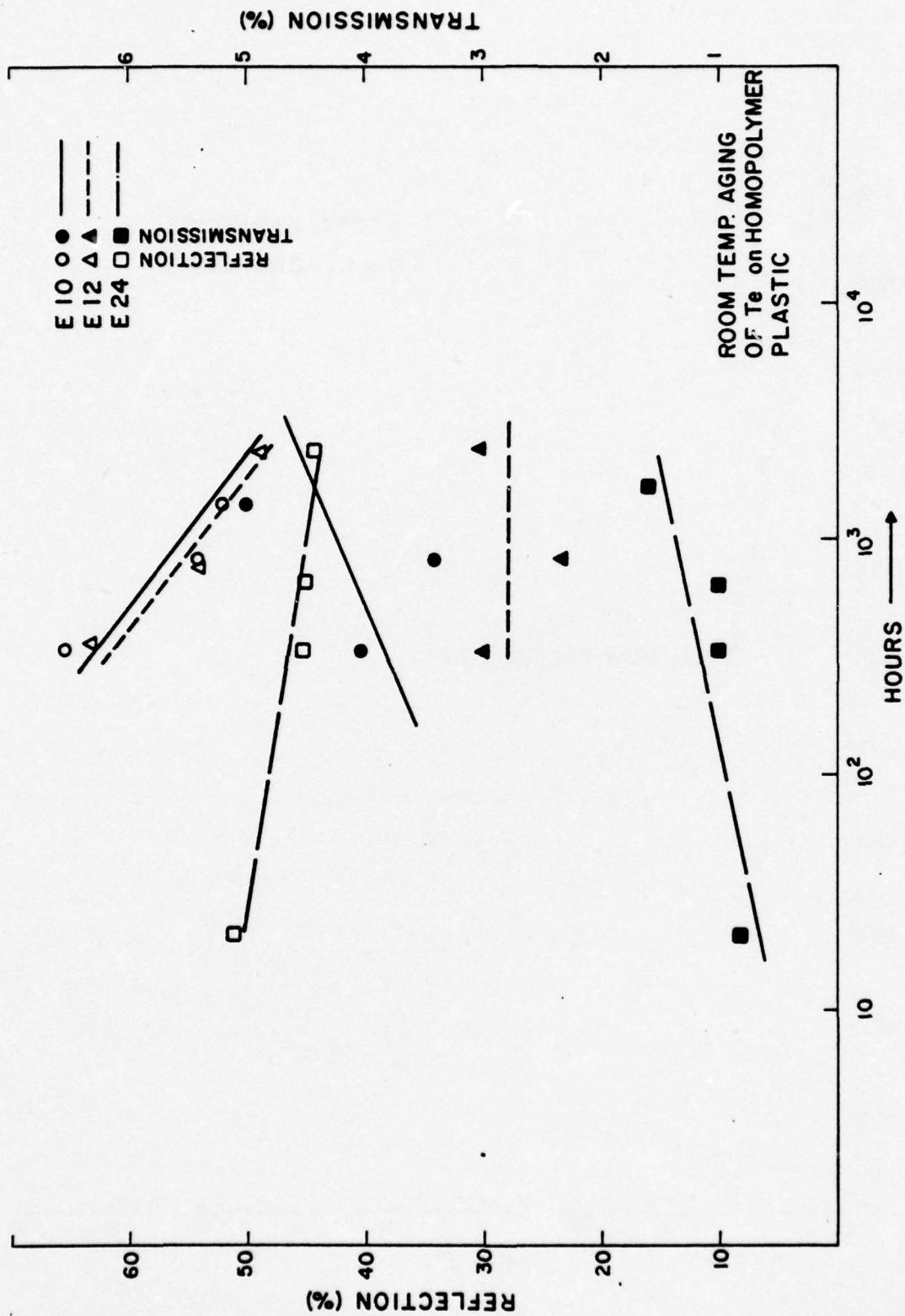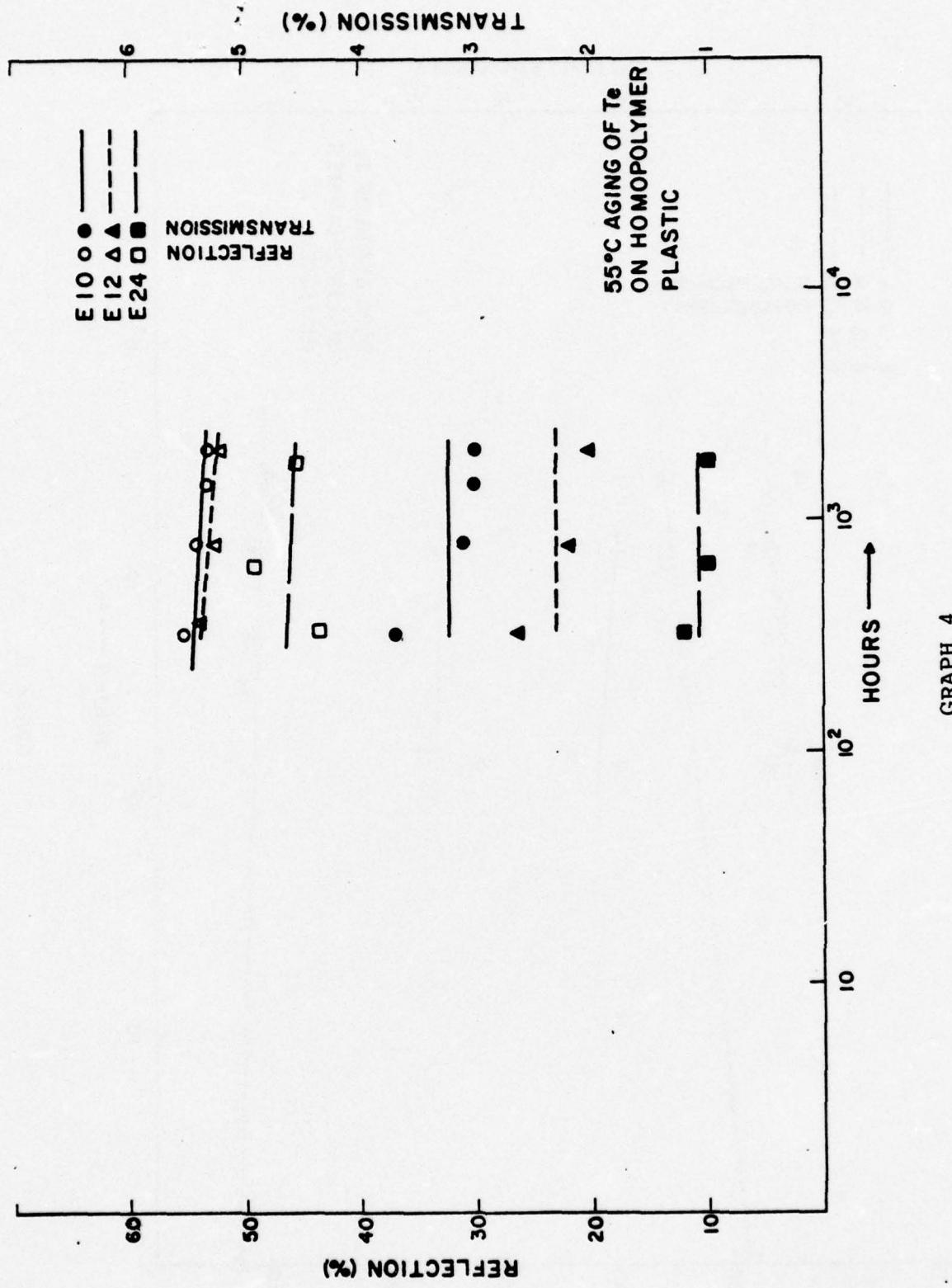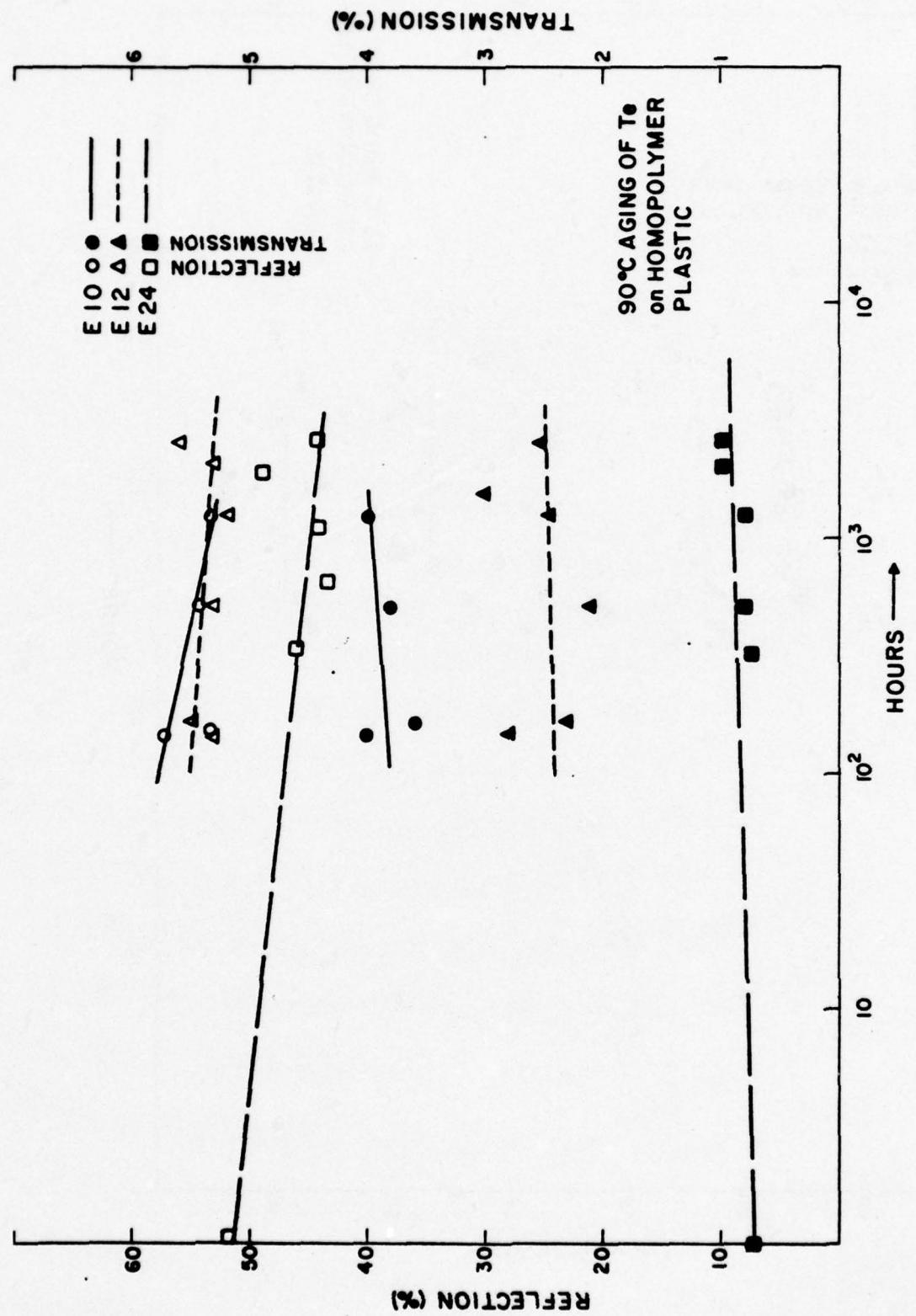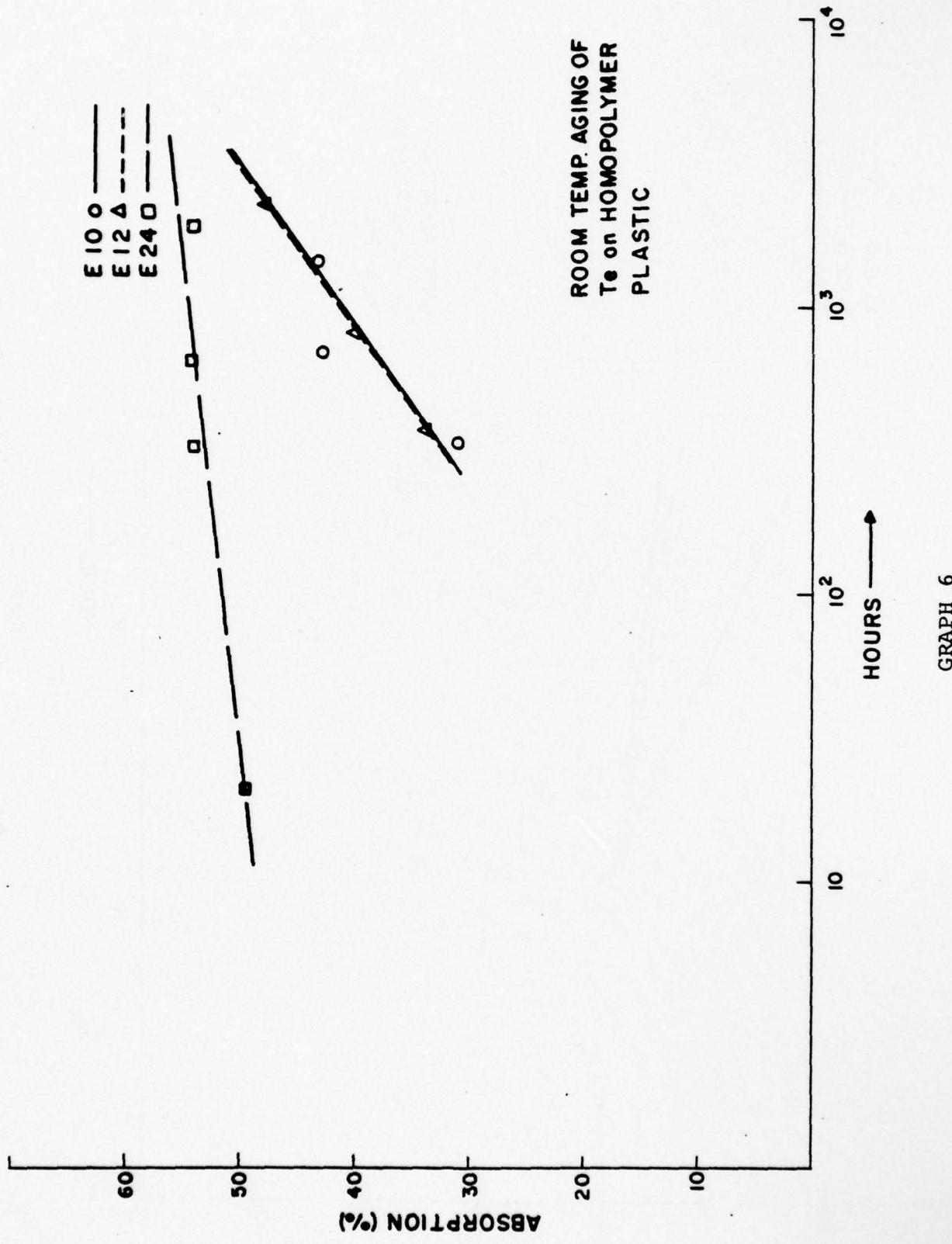
GRAPH 8
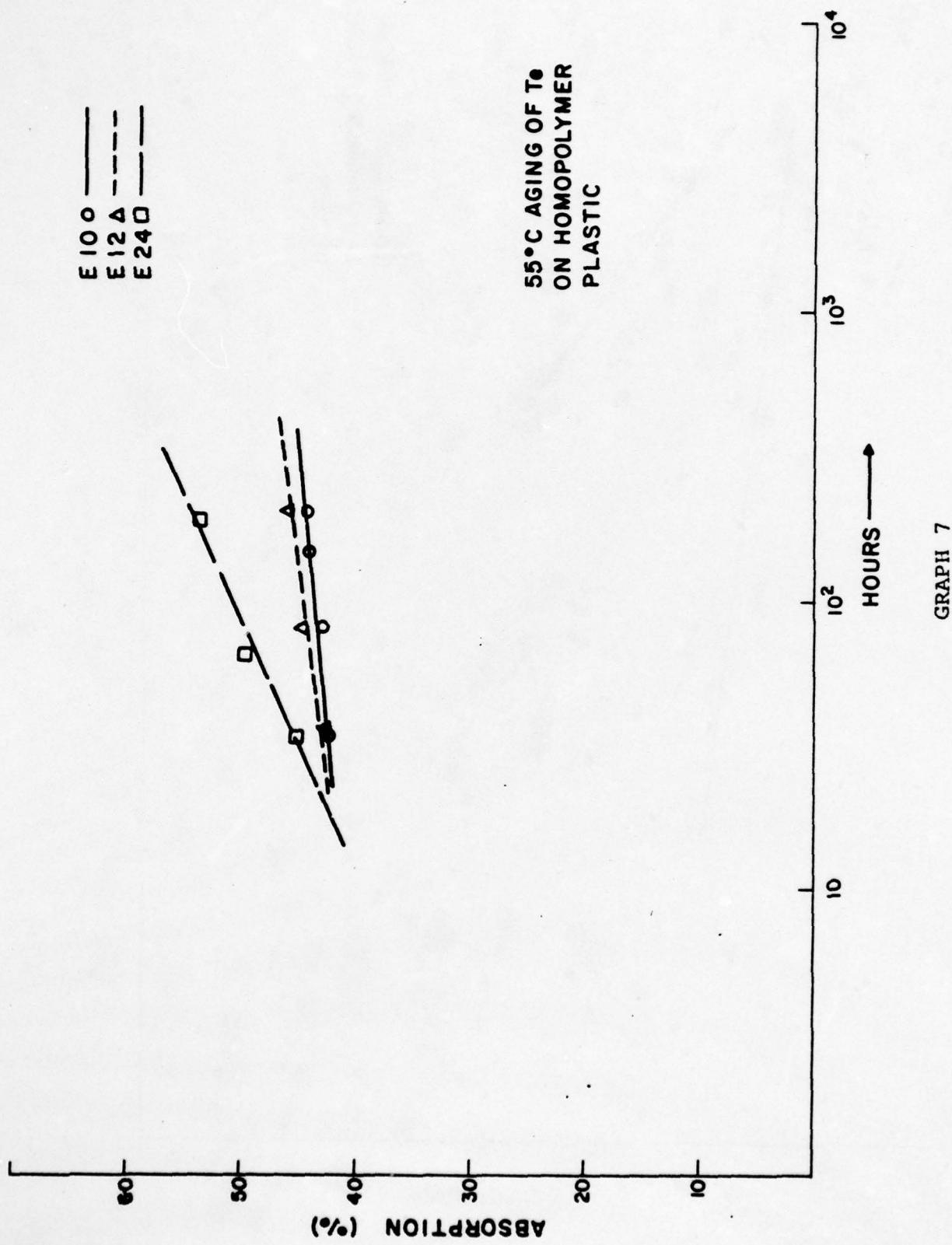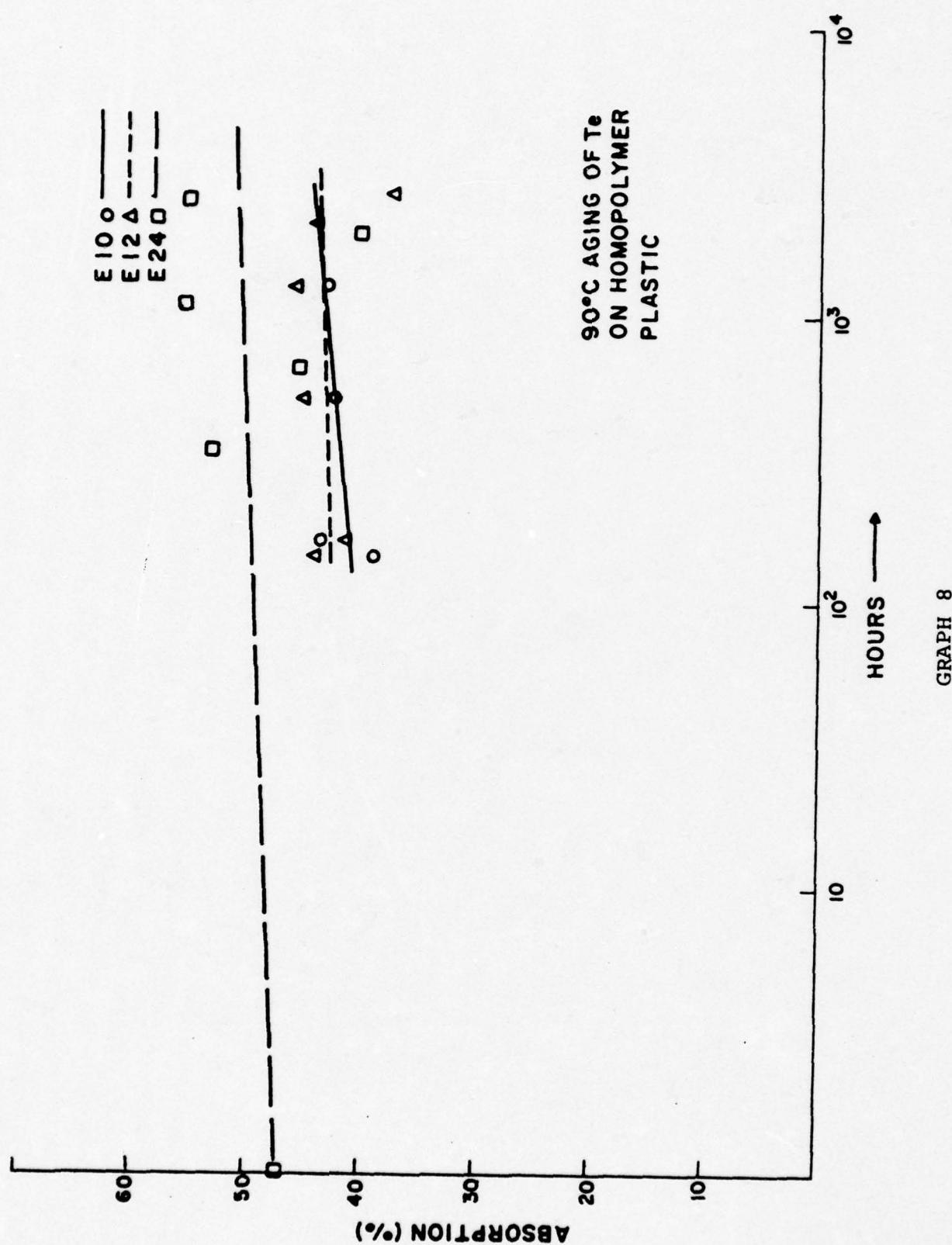
APPENDIX E

DRAW Disc Error Correction Coding and Modulation

by

Dr. Michael M. Goutmann

General Atronics Corporation
A Subsidiary of
The Magnavox Government and Industrial Electronics Company
Philadelphia, Pa. 19118

# DRAW DISC ERROR CORRECTION CODING AND MODULATION

## 1.0 INTRODUCTION

This report summarizes an approach to error correction coding and decoding, as well as a "modulation" approach to the DRAW disk. By modulation, we mean the way the bits are recorded in terms of pits, non-pits or transitiions between one state and the other. Although this function is itself called "coding" in magnetic recording literature, we shall adopt the communicators' terminology of modulation, reserving coding for the redundancy insertion to protect against bit errors during read-back.

Our model is then described in terms of Figure 1. The purpose of the interleaver is to protect against error bursts which are assumed to span as much as 256 bits. Hence an equivalent degree of interleaving is contemplated.*

---

*A burst "avoidance" mechanism will be described in another memorandum.

USER DATA → [ENCODER/INTERLEAVER] → [MODULATION] → [RECORDING/PLAYBACK] → [DEMODULATOR] → [DECODER/DEINTERLEAVER] → USER DATA
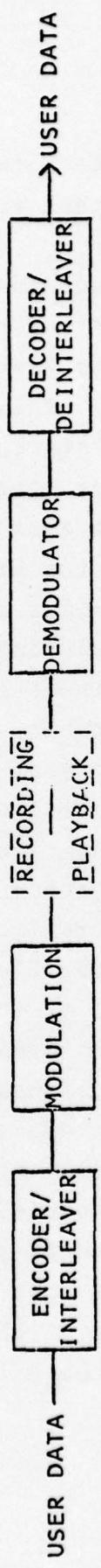
FIGURE 1

## 2.0    CHANNEL MODEL

By channel model we mean the mathematical mechanism which best duplicates the error pattern results of L. Vries and M. deHaan at Nat Lab.

Observation of the data leads to an error model mechanism shown in Figure 2. This error mechanism is controlled by the occurrence of missing non-pits (negative errors) rather than missing pits (positive errors). This model is useful in determining the probabilities of bursts containing a given number of errors. The error-to-error state transition in the model indicates the probability that another error will occur within a 2-microsecond window after the previous error occurs. It may be on successive bits, or on bits separated by as much as 13 bit intervals. An NRZ(M) modulation was used to determine the model. This effect upon these statistics for any other modulation must yet be established.

A side issue of the asymmetry of the channel, in that approximately ten times as many negative errors are made as positive errors, is the determination of an optimal input bit probability distribution. Since negative (e.g., 1→0) errors are more probable than positive errors (e.g., 0→1), it is conceivable that the data should favor 0's since fewer errors are made on them. On the other side of the coin, favoring one bit over the other reduces the information content of the data source, i.e., reduces the redundancy of the error correction code. The optimum values due to this compromise have been computed with the result that the zeroes should favor the ones by a probability of 0.502 to 0.498. The implication is that coding for the symmetric channel should be used to avoid complexity and that nothing is lost by doing this. The most interest-worthy consequence of this result is that the reader need not suffer through the arduous derivation proving the optimal distribution.
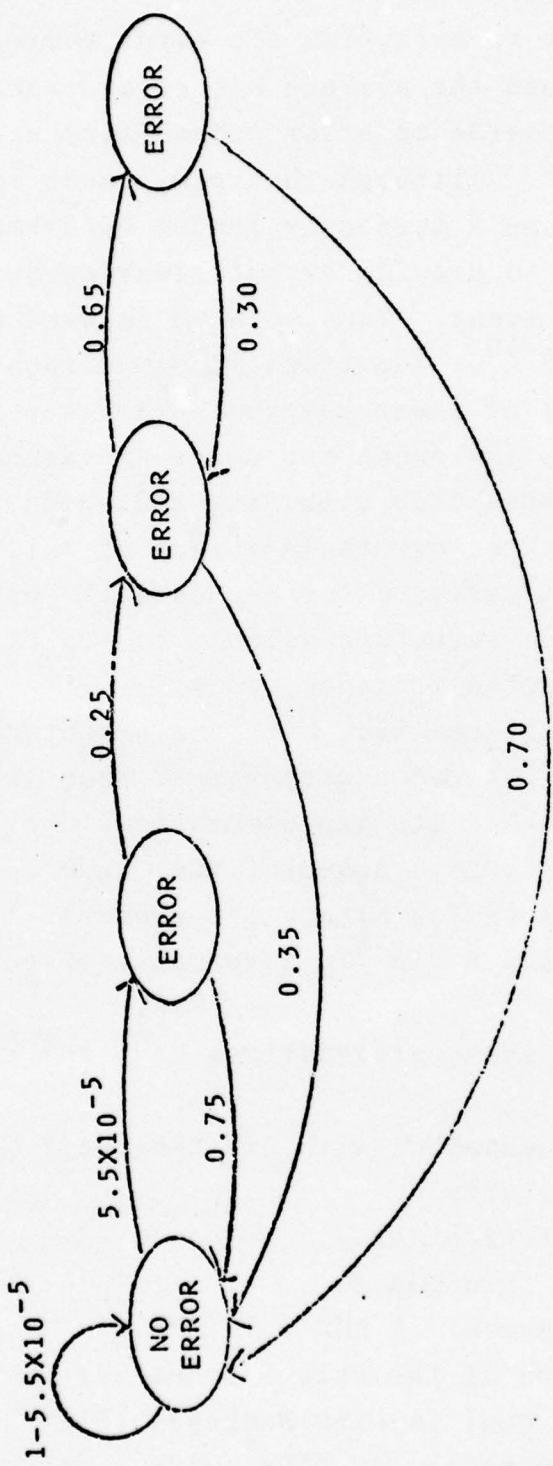
FIGURE 2

## 3.0 ERROR CORRECTION CODING

In order to establish the error correcting requirement of the code, we use the average bit error probability of $8 \times 10^{-5}$. The goal is to provide an error probability after decoding of better than $10^{-10}$. Although the requirement is $10^{-9}$, the computations assume a perfectly random occurrence of the errors which we attempt to provide by interleaving but which remains a probabilisitic event. Thus we have imposed a theoretical performance of $10^{-10}$. The codes at our disposal must be weighted in terms of their complexity and the speed of the circuitry used to implement the coder and decoder. We recommend a convolutional code with rate 1/2 which can correct all patterns of three errors in a span of thirty-six bits. The probability of error after decoding is approximately $5 \times 10^{-12}$. The code structure belongs to the class of self-orthogonal, perfect-difference codes.

A good alternative, with the advantage that it is a rate 2/3 code (50% redundancy rather than 100%), but with the disadvantage that its implementation takes at least twice the number of IC's, is a convolutional code which corrects all triple errors in 123 bits. The probability of error after decoding is $3.6 \times 10^{-10}$, given an average BER of $8 \times 10^{-5}$ before decoding.

Both of these alternatives have the following characteristics:
a) Easy implementation with off-the-shelf MSI and SSI (PMOS) digital circuits.
b) Easy synchronization
c) Continuous throughput
d) Operation speed: 1 kHz - 10 MHz

The implementation of the rate 1/2 decoder is estimated at approximately 30 Dual In-Line Packages (DIP) and the rate 2/3 decoder at approximately 60 DIPs, with a degree of interleaving of 256. With interleaving over 512, the count goes up to 40 and 100, respectively.

## 4.0    MODULATION

The requirement imposed in the modulation is primarily that of  zero DC value.  We recommend a modification to the Miller code which is expected to be similar to the $M^2$ code suggested by Mallison and Miller.*

Since the authors carefully avoid the description of the $M^2$ code (modulation to us), a direct comparison is impossible.  The authors, however, mention that their code produces transition-free runs of 2-1/2 and 3 data intervals. The generation we proposed leads to transition-free runs of 2-1/2 but none of 3.  The reader is  requested to draw up his own conclusions.

The idea is to modulate the information in such a manner as to guarantee a short-term zero DC average. Starting with the Miller coding, we look upon a digital sequence as being made up of a concatenation of subsequences of the following types

> a) 011...10
> b) 11...1

where sequences of type (a) are run lengths of n ones, where $n \geq 0$, sandwiched between two zeroes (run lengths of zeroes fit in this type in pairs).  Type (b) corresponds to sequences which have n ones.

According to Miller coding, only sequences of type (a) with n even and non-zero have non-zero DC value.  It is, therefore, those sequences which are modified.

Let us define the following rules of waveform generation:

- a will correspond to *no* transition (delayed) in the data interval;
- b will correspond to a transition in the middle of the data interval;

---

*J.C. Mallison and J.W. Miller, "On Optimal Codes for Digital Magnetic Recording," Conference on Video and Digital Recording, Birmingham, AL, 20-22 July 1976.

77

c will correspond to a transition at the end of the data
interval.

Figure 3 then describes the encoder as a state diagram.
An example best summarizes this formal procedure and is
presented in Figure 4. The only modification in the modulation
of the sequence on Miller Coding is at the end of the first
run length of ones. The sequence can be represented as the
concatenation of the following subsequences:

$$0 \; 0$$
$$0 \; 1 \; 1 \; 1 \; 1 \; 0$$
$$0 \; 1 \; 1 \; 1 \; 0$$
$$1 \; 1 \; 1 \; 1$$
$$0 \; 0$$
$$1 \; ...$$

Demodulation takes on a similar Markovian structure.
The detection parameters are

   $t$ - Transition in the middle of the data interval

   $\Delta$ - No transition during the data interval but a transition
relative to the previous data interval (only if it
was not a $t$ interval)

   $\overline{\Delta}$ - No transition during the data interval and no transition
relative to the previous data interval.

Because of the memory in the modulation, a delay will
exist in the demodulation. Hence every time a detection
statistic $(t, \Delta, \overline{\Delta})$ is tested, the decision may have to be
delayed. This is indicated in Figure 5 by a $\phi$ output indi-
cation.

A problem in demodulating with memory (feedback) is
that of error propagation. Can any sequence of errors put
the demodulator (true of error correction decoding as well)
in a state from which errors will be generated by a sequence
of permissible states in the sequential structure even though
channel errors do not occur? Since a return to state 1 is
guaranteed in at most three data intervals, there is zero
probability of being trapped in a subcycle of the Markov
chain. Furthermore, the error burst due to the modulation
cannot last more than three bits.

a = NO TRANSITION (DELAYED TRANSITION)

b = TRANSITION IN MIDDLE OF DATA INTERVAL

c = TRANSITION AT END OF DATA INTERVAL

X = ANYTHING

FIGURE 3

ENCODER

0 0 0 1 1 1 1 0 0 1 1 0 1 1 1 1 0 0 1

c c a b b c a c a b b a b b b c a b

MODULATOR SEQUENCE

Δ Δ Δ t t Δ̄ Δ Δ Δ t t t̄ Δ t t̄ · t t̄ Δ t

φ (000) 1 1 φ (110) φ (01) 1 1 φ (01) 1 1 φ (01) 1 1 φ (001)

DEMODULATOR SEQUENCE
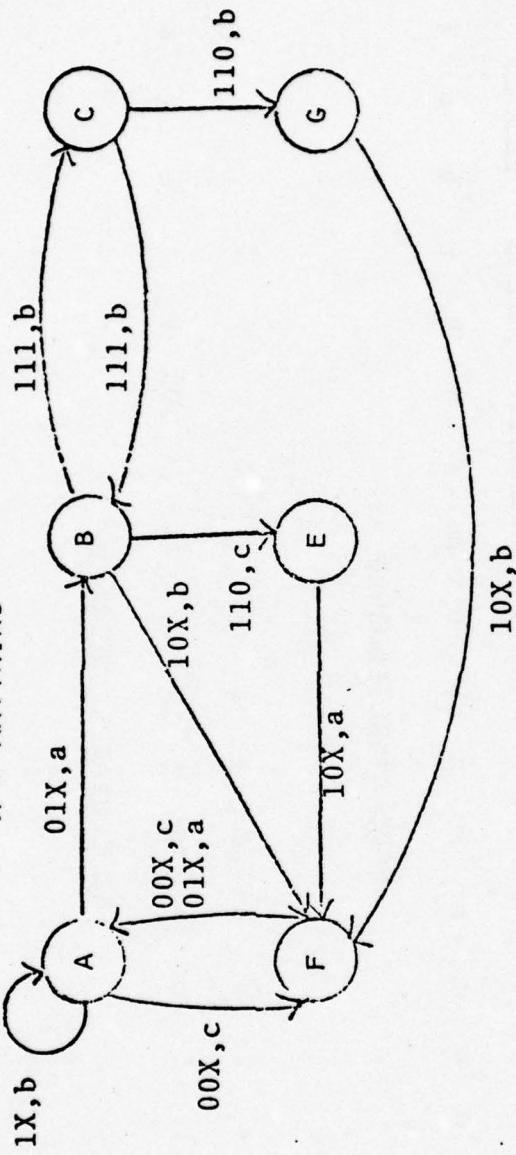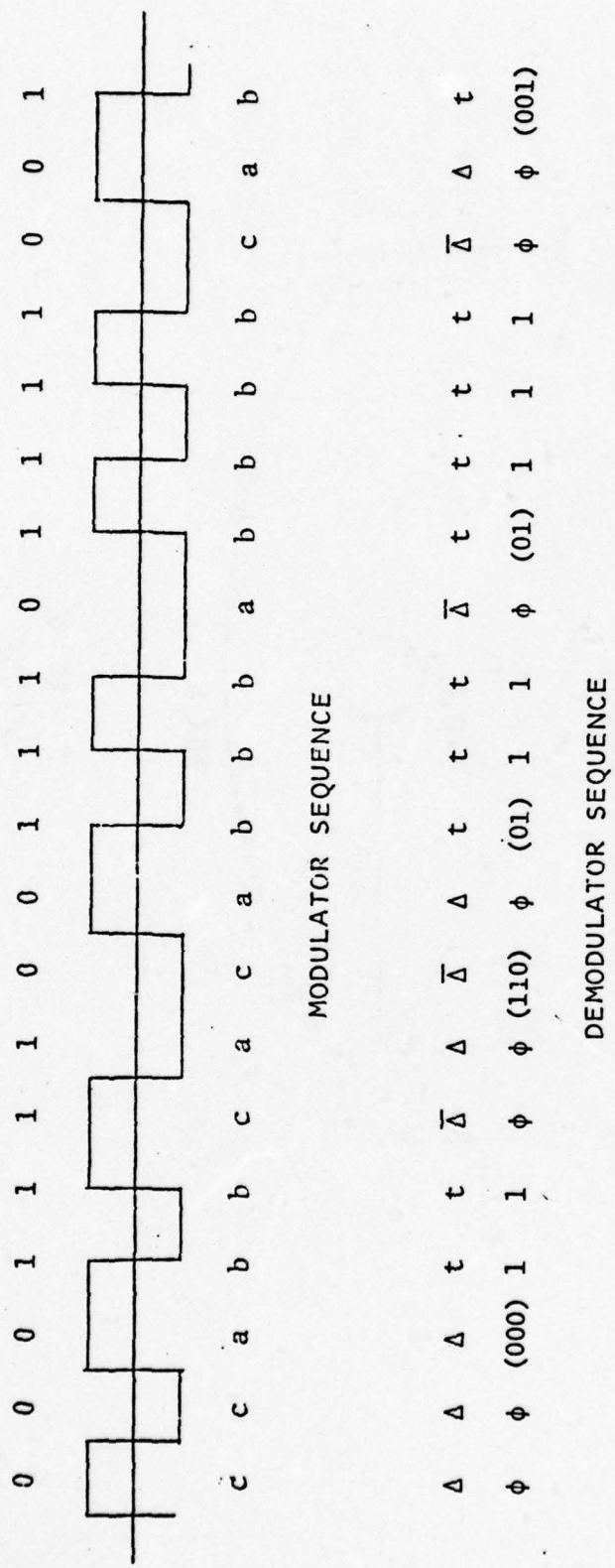
FIGURE 4

EXAMPLE
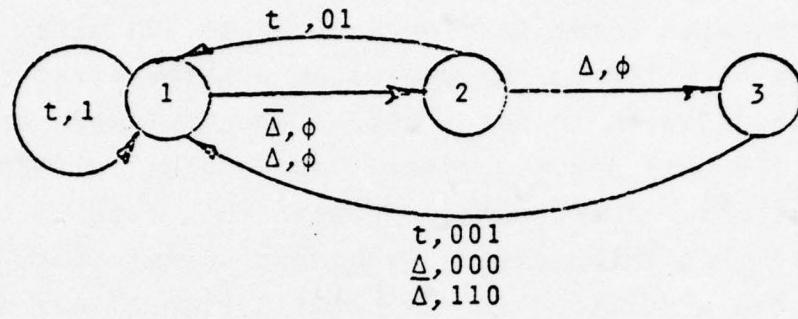
FIGURE 5
DEMODULATOR

## 4.0    CONCLUSION

We have generated so far a structure which serves the goals of error correction coding so that an error rate in the order of one in $10^{10}$ bits can be realized in spite of a burst error structure which exhibits approximately one burst in $2 \times 10^4$ bits, with burst lasting as long as 300 bits.   These statistics have led to the choice of a three-error correcting code.  The decision to use a self-orthogonal code was due to speed (10 MHz) and implementation complexity ($\sim$30 DIPs) considerations.  The bookkeeping with this type of code, especially when interleaved, is almost nonexistent.

The modulation (modified Miller code) was dictated by the requirement of zero DC waveform (short-term) and the advantage of minimizing run lengths (2-1/2 data periods), thereby providing the system with a good clock extraction capability (VCO at twice the bit rate).

Another memorandum will describe a method whereby the immediate Read-After-Write capability is used to eliminate (and rewrite) areas of the disk where errors are found on read-back.

APPENDIX F

Disc Data Formating Employing Soft Sectoring

by

Ray Hunt

The Magnavox Government and Industrial Electronics Company
Philadelphia, Pa. 19118

## DISC DATA FORMATING EMPLOYING SOFT SECTORING

### Introduction

Rotating magnetic memories represent the more popular tool for mass, high speed retrieval of data for computers. Data is organized in an orderly fashion on such devices by cylinders (tracks) and sectors. Each track is defined as a cylinder having a unique radial location on the rotating media. Each sector is defined by a physical mark on the media, either a hole punched on the media itself, or a slot in an index device attached to the media. Such a method of defining sectors is referred to as "Hard Sectoring". This letter will describe a method of data storage which employs no physical sector marks or index holes, a method referred to as "Soft Sectoring".

### Soft Sectoring Description

Soft sectoring is a method of data storage on a rotating mass memory device that employs neither sector marks nor index holes to define individual blocks of data, called sectors, on cylinders of data containing a number of sectors, such cylinders called tracks. Employment of such a sectoring method lays the burden of sector location on the data itself, not on physical marks or holes, thus eliminating the need of the electronics necessary to detect the indexing marks or holes. This technique requires that each sector contain its characteristic sector address in an address block or "Label" preceding the data in order to establish such a sector address. The assumption is made that the data itself is recorded in a synchronous fashion such that the start of a block of data is defined by a sync word utilized to establish bit sync preceded by a guard band utilized to insure separation of blocks of data.

## Data Formats

Individual records (sectors) of information may be defined in such a fashion to contain its own characteristic address, a fixed length of block of data, and sufficient error correction and detecting techniques to provide reliable data, together with sufficient guard bands preceding and following the data to insure block separation. Such a method is shown in Figure 1. This method employs 6 discrete fields of data: a) preamble b) sync word c) label d) data e) cyclic redundancy check character f) postamble.

### A) Preamble

The preamble is a guard band preceding the sync word that insures the separation of the present data block from the previous data block. This guard band consists of a string of binary Zeros. Although this guard band may be of any length, experience has shown that a length of approximately 1/16 the data length insures separation.

### B) Sync Word

The sync word is a sequence of binary bits utilized to establish bit synchronization and define the start of data within the data block. This sync word should be of relatively unique and not follow the rules of error detection and correction employed by the data section such that the sequence would be unlikely to be found in that section. One such sync word is an 11 - bit Barker sequence (11100010010).

### C) Label Field

The label field of the data block contains the address of the soft sector and a least significant portion of the track address. Since

both track and sector address information are included, assurity is
given that the proper data can be located despite track positioning
inaccuracies. The label field is subject to all error detection and
correction techniques employed within the data field described below.

D) Data Field

The Data Field is a block of data of fixed length containing the data
to be retreived. This field will contain a convenient $2^{nth}$ number of
bytes of data. The bites of data will contain 8 bits of usable data
since this is a least common multiple of data that could be demanded
by 16, 24, or 32 bit computers. Error detection and correction tech-
niques would be employed on such bytes to improve the data reliability.

E) Cyclic Redundancy Check

The cyclic redundancy check character is a 16 bit (2 byte) data word
subject to error detection and correction that verifys the corrected
data field previously received. As the corrected data is received,
a polynomial is formed, such that the inclusion of this check character
into the polynomial will result in a test to prove the data was read
correctly. Such polynomial generation and testing may be implemented
with commercially available devices designed for just such a task.

F) Postamble

The postamble is a guard field much the same as the preamble, insuring
record separation. The length of such a field, however need not be
as long as the preamble. Experience has shown that a postamble half
the length of the next preamble is desirable.

86

## EXAMPLES

Below are illustrated several examples of the employment of the above techniques. Rotating memories store data in contiguous section locations. Since a sector is the least common factor of the data size, consideration is given to insure that the data block is large enough to minimize the overhead implied by labels and guard bands, yet small enough to insure that a minimal spare will be utilized for a wide range of data lengths to be retreived. The most common format provides 256 8 bit bytes in the data field.

In the examples below the data field will be varied resulting in a number of sectors per track with the assumption of there being $4.4 \times 10^5$ bits per track. In each case the preamble is chosen to be approximately 1/16 the data field and the postamble 1/2 the preamble. The sync, label, and CRC fields are held constant at 63 bits (a Barker sequence sync, 2 bytes each for label and CRC employing (13, 5) error correcting code). The total number of possible sectors is factored by 20% to give a minimum of 20% spare tracks. This is done to allow for errors in writing data. (If an error is made in writing a sector, it may be marked defective, and the sector re-written in a spare track). An efficiency factor is then derived from the number of usable data bits per track divided by the total possible bits per track.

1)  Assume 2048 Data Bytes/Sector

| | | |
|---|---|---|
| Employ (13, 5) ECC Yields | 26624 | Raw Data Bits |
| Sync + Label + CRC | 63 | RDB |
| Preamble | 1600 | RDB |
| Postamble | 800 | RDB |
| | 29087 | Bits/Sector |

87

$4.4 \times 10^5$ Bits/Track

_____

29087 Bits/Sector          15 Sectors/Track

Possible configuration       12 Usable Sectors

                                             3 Spare Sectors

Efficiency Factor

$$\frac{2048 \text{ Byte/Sector} \cdot 8 \text{ Bits/Byte} \cdot 12 \text{ Sectors/Track}}{4.4 \times 10^5 \text{ Bits/Track}} = .45$$

2)   Assume 256 Data Bytes/Sector

     Employ (13, 5) ECC Yields      3328   RDB

     Sync + Label + CRC          63   RDB

     Preamble                      200   RDB

     Postamble                   100   RDB

                                         3690   Bits/Sector

$4.4 \times 10^5$ Bits/Track

_____                119 Sectors/Track

3690 Bits/Sector

Possible configuration       100 Usable Sectors

                                         19 Spare Sectors

Efficiency Factor

$$\frac{256 \text{ Byte/Sector} \cdot 8 \text{ Bit/Byte} \cdot 100 \text{ Sector/Track}}{4.4 \times 10^5 \text{ Bits/Track}} = .47$$

3) Assume 64 Data Bytes/Sector

Employ (13, 5) ECC Yields                     832 RDB

Sync + Label + CRC   =               63 RDB

Preamble              =               50 RDB

Postamble            =           <u>25 RDB</u>

                                967 Bits/Sector

$$\frac{4.4 \times 10^5 \text{ Bits/Track}}{967 \text{ Bits/Sector}}$$         455 Sectors/Track

Possible Configuration         380 Usable Tracks

                                75 Spare Tracks

Efficiency Factor

$$\frac{64 \text{ Byte/Sector} \cdot 8 \text{ Bit/Byte} \cdot 380 \text{ Sector/Track}}{4.4 \times 10^5 \text{ Bits/Track}} = .44$$
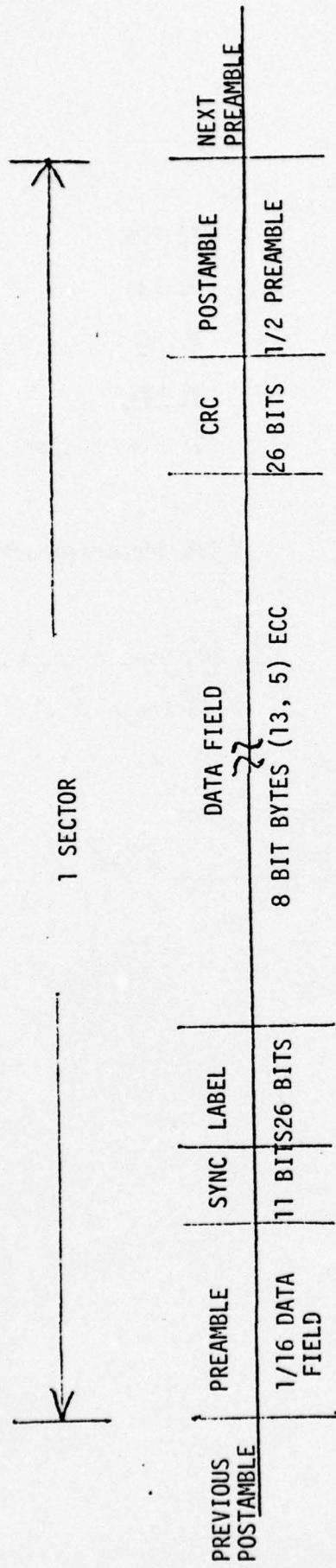
SOFT SECTOR DATA FORMAT

FIGURE 1

90

APPENDIX G


DRAW Recording Experiments on Tellurium Films

by

D. Lou
D. Stanton
M. Strzelczyk

## DRAW RECORDING EXPERIMENTS ON TELLURIUM FILMS

### 1. SUBSTRATE PREPARATION

Typical DRAW recording experiments were carried out on glass masters supplied by N.V. Philips and on PMMA discs supplied by MCA and Glasflex. The standard cleaning procedures were:

- Rinse with distilled water.
- Soak in detergent (alkanox) solution.
- Rinse in distilled water.
- Blow dry with nitrogen.

Uniform deposition over the 30 cm diameter substrate area was achieved using the technique first developed by Behrdt. This is illustrated in Figure 1. The disc is placed at a height of
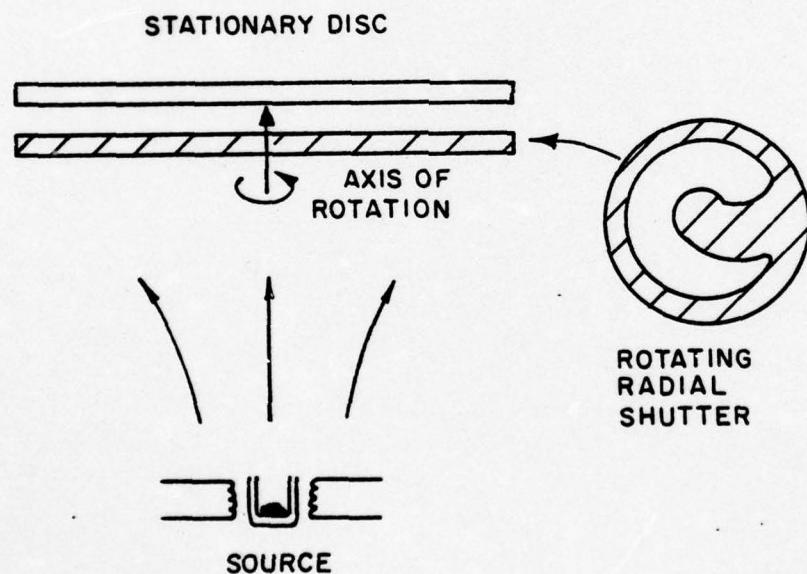


Figure 1: Technique for uniform large area deposition.

about 50 cm from the source. Uniformity in the azimuthal direction is achieved by locating the source at the center of the disc. Uniformity in the radial direction is achieved by

rotating a compensating shutter of the properly designed shape underneath the disc. Figure 2 shows the nonuniformity in the thicknesses and optical transmission of tellurium films deposited by this technique. It appears that thickness homogeneity better than ± 3% has been achieved. The evaporation was carried out in a Varian 3117 vacuum evaporator. Film thicknesses and deposition rates were monitored by means of an Inficon XMS-3 programmable quartz crystal thickness monitor. Deposition conditions were similar to those listed in the previous quarterly report.

## 2.     LASER MACHINING

A Spectra Physics Model 165 argon laser lasing at 488 nm was used for writing. Modulation was provided by a Coherent Associates Model 3025 electro-optic modulation system. Typically, the modulator was operated with a through-put transmission of 60%, an extinction ratio of better than 50 to 1, a duty cycle of approximately 50%, and a 3 dB bandwidth of 28 MHz. The deflected light from the modulator is monitored by means of a photodiode.

After the modulator, the light is then attenuated to the proper power level by a neutral density variable attenuator. The beam is then directed onto the optical subsystem which moves on an air bearing sled towards the circumference of the rotating disc. The beam is focused by a spot lens and reflected off the dichroic mirror into the recording objective. For recording through the substrate, the objective was custom designed by Cerco with 30X magnification, 0.55 numerical aperture, and working distance of 0.2 mm of air and 1.5 mm of plastic. Field lenses of various focal lengths were used. The different degree of filling for the recording objective leads to different power density profiles in the writing spot. These profiles are measured by the technique described in Appendix A. The typical writing spot has a full width half maximum diameter of between 0.6 µm to 1 µm.
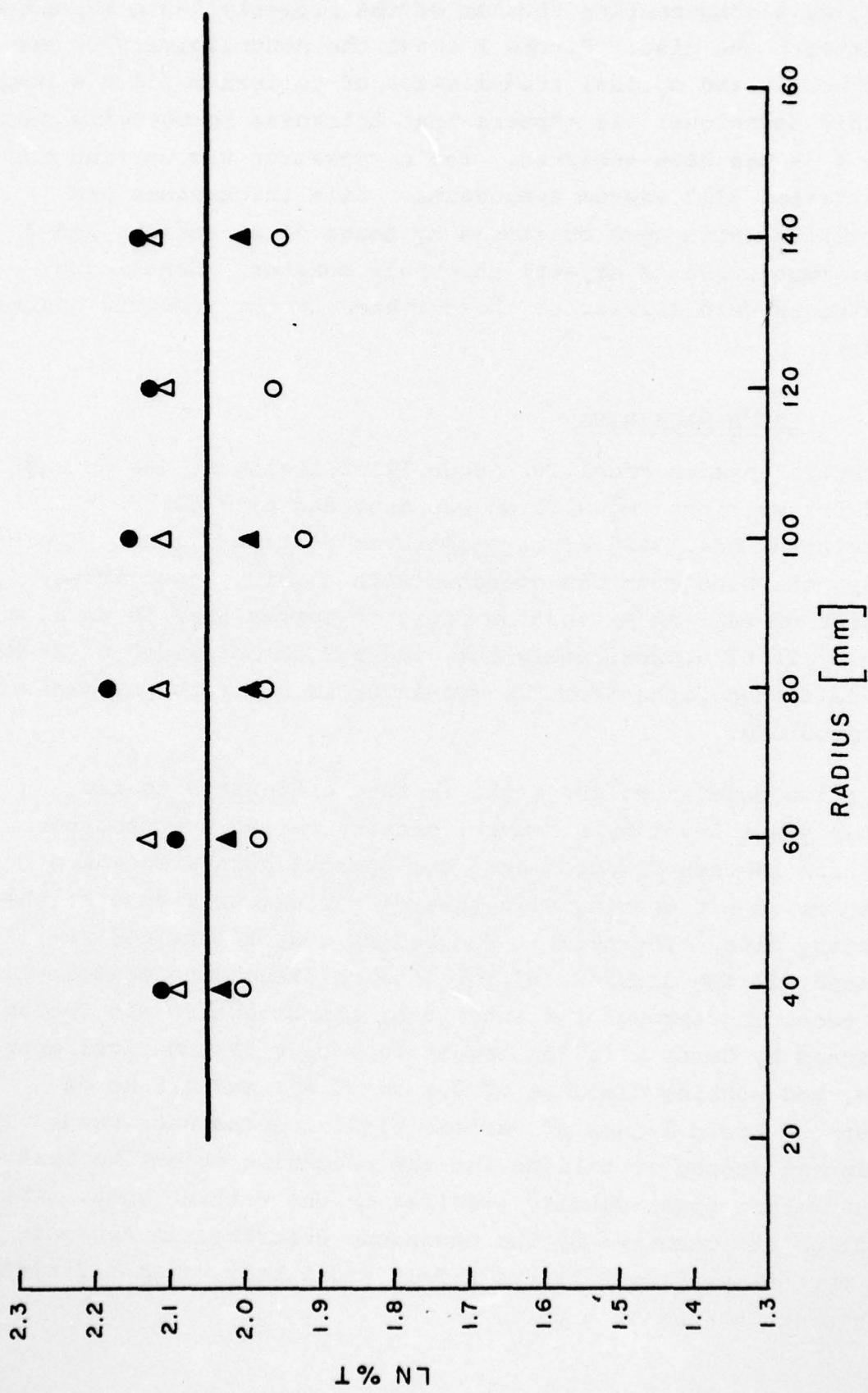
Figure 2a: Thickness distribution of deposited tellurium films.
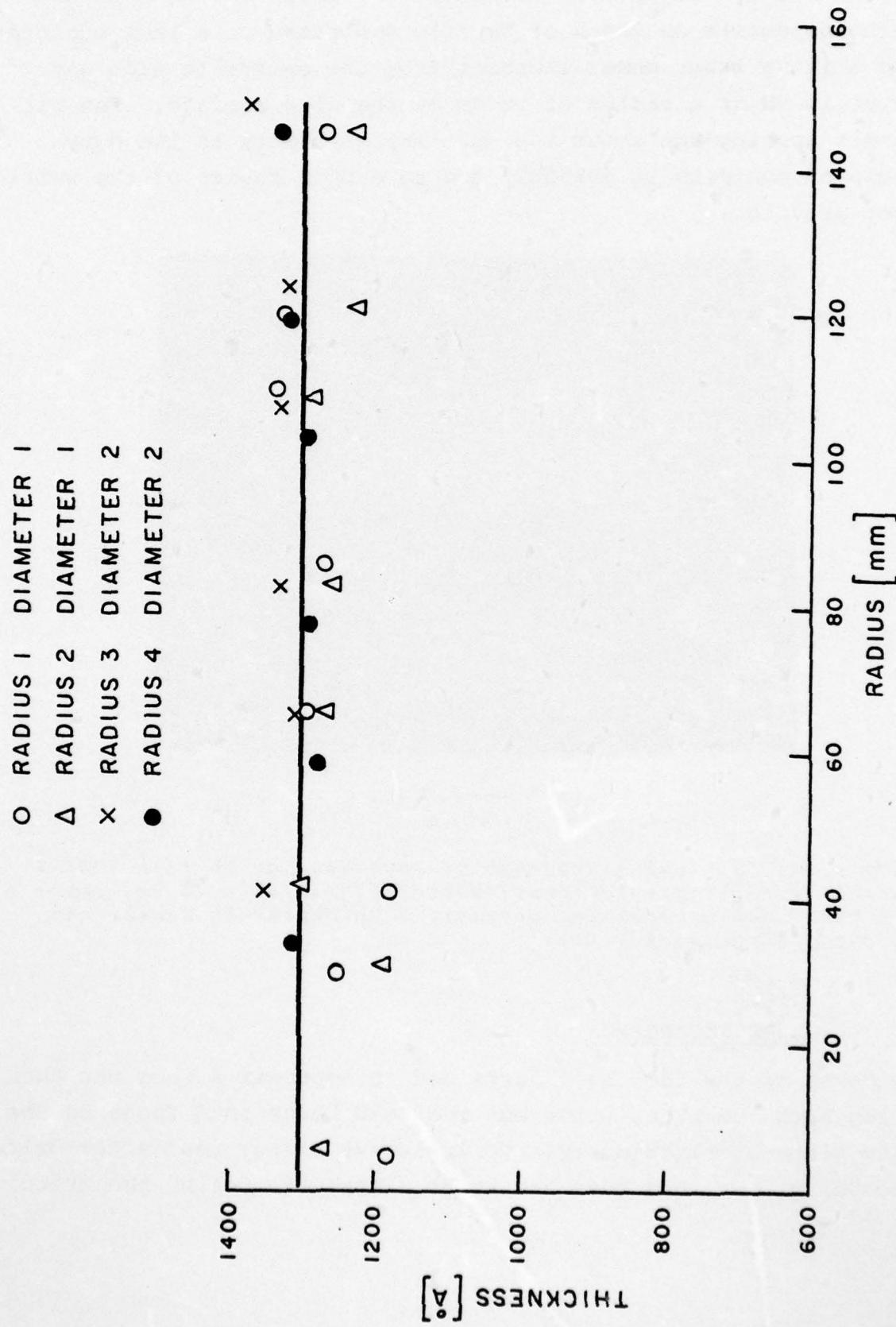
Figure 2b: Optical transmission (633 nm) of deposited tellurium films.

Figure 3 shows an optical micrograph of pits written with the Cerco objective on 250 Å of Te film deposited on a PMMA substrate. The writing laser power incident from the substrate side was about 15 mW at a radius of 10 cm on the disc surface. The pit-to-pit spacing was about 1.8 μm. The asymmetry in the duty cycle of the pits is probably due to a poor choice of the writing spot profile.



10 μm
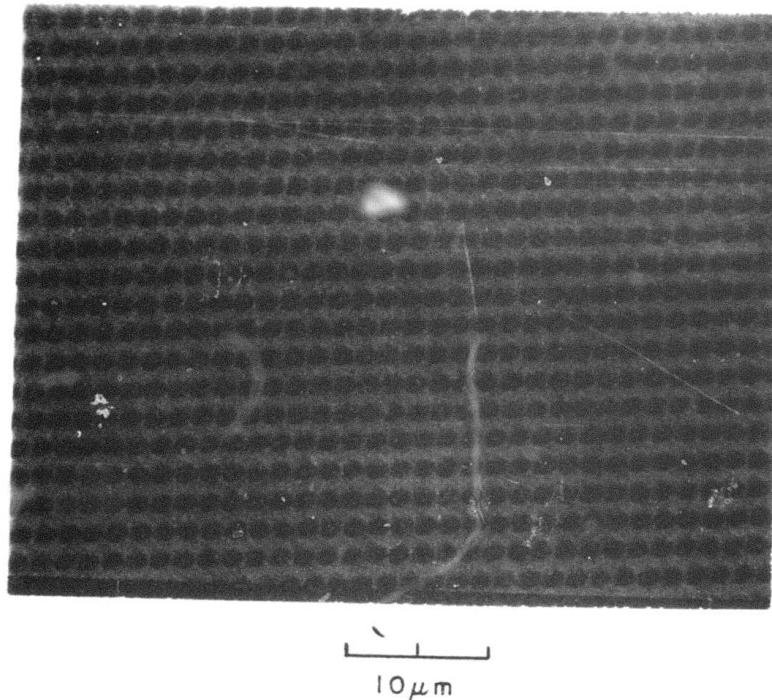
Figure 3a: Optical micrograph of recording on Te film (250 Å thick), a substrate incident recording, radius = 10 cm, power = 15 mW, 10 MHz unmodulated carrier, 2 μm center to center pit spacing, 2 μm track pitch.

3.    DRAW RECORDING

By means of the technique described in Appendix A, one can then bring both the blue, write and red read beams into focus on the disc plane simultaneously. To implement direct read after write recording, the read beam has to be aligned to follow the write
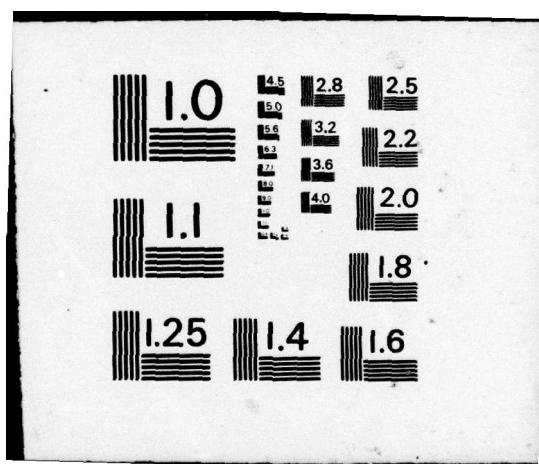
beam. Figure 4a shows the frequency spectrum of the DRAW signal from a tellurium (250 Å) film on PMMA substrate. The spectrum analyzer has a sweep width of 30 kHz, a horizontal scale of 2 MHz per division, and a vertical scale of 10 dB per division. The amplitude of the signal detected was 30 mV peak-to-peak at the diode, the frequency was 10 MHz, and the signal-to-noise ratio was better than 30 dB. The laser beam was incident from the substrate side through 1 mm of PMMA.

No radial tracking was attempted in the DRAW mode. Optimum DRAW signal was observed with a power level at the disc surface of 10 mW at the inner radius of 6 cm and 20 mW at the outer radius of 14 cm. DRAW was confirmed by blocking off the write beam. The signal disappears immediately, as shown in Figure 4b.
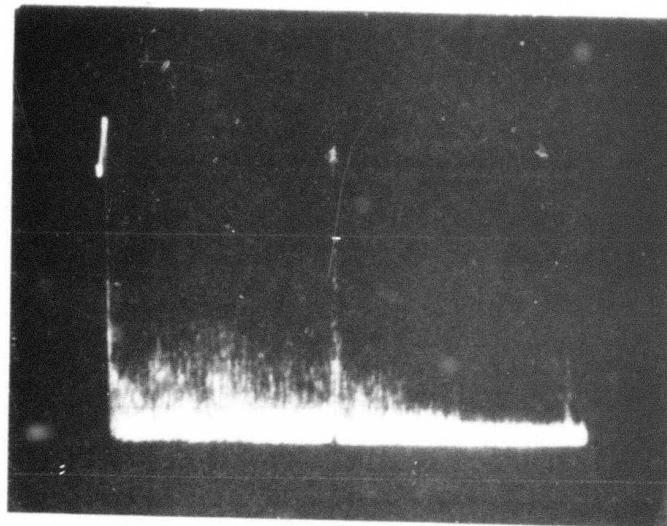
Figure 4a: Frequency spectrum of direct read after
write signal from tellurium disc.  Spectrum analyzer
sweep width 30 kHz, 2 MHz per division horizontal scale,
10 dB per division vertical scale.  Defected signal
was 10 MHz single frequency and 30 dB over noise.
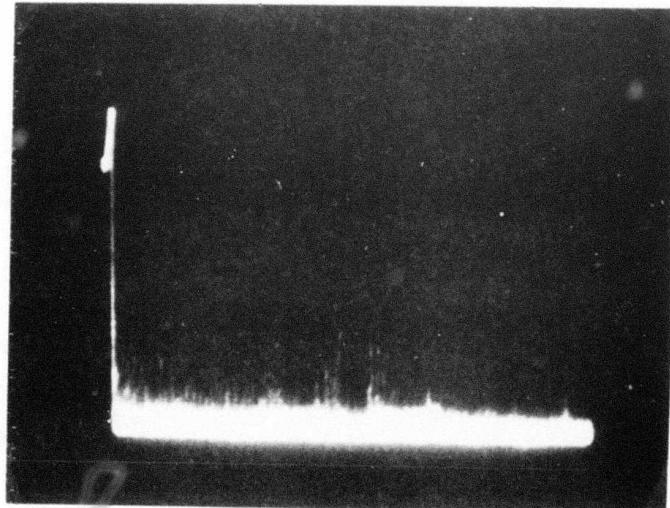


Figure 4b:  The same spectrum when the write beam was
blocked off.